이학박사 학위논문

Biomolecule-Carbon Nanotube Hybrid Structures for the Monitoring of Sensory Receptor Activity and Their Application to Bioelectronic Sensors

감각 수용체의 작용을 연구하기 위한
바이오분자-탄소나노튜브 융합 구조 및
바이오전자 센서로의 응용

2019 년 2 월

서울대학교 대학원

물리천문학부 물리학 전공

이 민 주

Biomolecule-Carbon Nanotube Hybrid Structures for the Monitoring of Sensory Receptor Activity and Their Application to Bioelectronic Sensors

by

Minju Lee

Supervised by

Professor Seunghun Hong

A Dissertation Submitted to the Faculty of Seoul National University in Partial Fulfillment of the Requirements for the Degree of Doctor of Philosophy

February 2019

Department of Physics and Astronomy

Graduate School

Seoul National University

Abstract

Biomolecule-Carbon Nanotube Hybrid Structures for the Monitoring of Sensory Receptor Activity and Their Application to Bioelectronic Sensors

Minju Lee

Department of Physics and Astronomy

The Graduate School

Seoul National University

Human recognizes various odorants and tastants through olfactory and gustatory systems. The senses of smell and taste are triggered when sensory receptors in cells receive chemical signals from outside cells. That is, sensory receptors work as first sensing parts in sensory systems. Thus, the monitoring of sensory receptor activity is crucial for the fundamental understanding of sensory systems. In addition, the study on sensory receptors can lead to the development of bioelectronic sensors. In this dissertation, it will be discussed about the electrically monitoring of sensory receptor activity via bioelectronic sensors. The bioelectronic sensors were based on carbon nanotube field effect

transistors (CNT-FETs) with gold floating electrodes, resulting in enhanced sensor sensitivity and selectivity.

First, a bioelectronic tongue based on nanovesicles for the monitoring of honeybee gustatory receptor activity to umami taste will be discussed. Here, CNT-FETs with floating electrodes were hybridized with nanovesicles containing honeybee umami taste receptor, gustatory receptor 10 of *Apis mellifera* (AmGr10). This strategy enabled us to discriminate between L-monosodium glutamate (MSG), best-known umami tastant, and non-umami substances with high sensitivity and selectivity. Interestingly, it could also be utilized for the detection of MSG in liquid foods such as chicken stock. Moreover, the enhancement of umami taste sensation by an enhancer material (disodium 5'-inosinate, IMP) was demonstrated using this platform.

Next, a bioelectronic nose based on nanodiscs (NDs) for the monitoring of human olfactory receptor activity to a rose scent will be discussed. In this strategy, a floating electrode-based CNT-FET was functionalized with human olfactory receptor 1A2 (hOR1A2)-embedded NDs (hOR1A2NDs). This strategy allowed us to quantitatively assess the contents of geraniol and citronellol, the main components of a rose scent, as low as 1 fM and 10 fM, respectively. Importantly, we also demonstrated that the responses of hOR1A2NDs

to a rose scent could be strongly enhanced by an enhancer material like a human nose. Furthermore, the method provided a means to quantitatively evaluate rose scent components in real samples such as rose oil.

Keywords: sensory receptor, nanovesicle, nanodisc, carbon nanotube field effect transistor, floating electrode, bioelectronic sensor

Student Number: 2013-20376

Table of contents

List of figures

Chapter 1

Introduction

1.1 Membrane Receptor

Five senses are closely associated with a human life. Above all, human recognizes various odorants and tastants through olfactory and gustatory systems, allowing us to perceive important information about our surrounding. The senses of smell and taste are triggered when sensory receptors in cells receive chemical signals from outside the cells. Various receptor proteins embedded in the plasma membrane of cells allow communications between inside and outside of the cells [1]. Signal transduction is trigged through these membrane receptors. G protein-coupled receptors (GPCRs) are the largest group of membrane receptors, and they are involved in physiological processes such as sensory and hormonal signaling. When a specific ligand binds to a GPCR, it induces a conformation change in the receptor. The conformation change activates G protein, and it triggers signal transduction [2-4]. Ion channel-linked receptors which is other group of membrane receptors open to allow ions to pass through membrane in response to the binding of ligands [5]. These membrane receptors exist especially in olfactory and gustatory systems [4]. They have been widely studied because they can provide fundamental understanding of sensory systems. In addition, the study on sensory receptors can lead to the development of bioelectronic sensors.

1.2 Monitoring of Receptor Activity

Previously, the monitoring of receptor activity has mainly conducted by cell-based assays. For example, in the case of a fluorescence assay, cells expressing certain receptor proteins are cultured and treated with fluorescence indicators. Then, the receptor activity can be monitored by measuring a fluorescence intensity [6]. In the case of a luciferase assay, receptor proteins and luciferase gene are transfected in cells. When ligands bind to the receptor proteins, signal transduction is initiated, which results in the expression of luciferase gene [7]. The receptor activity can be monitored by measuring a luminescence intensity in cells. However, they are difficult and complicated methods to manipulate. In addition, it is hard to sensitively monitor receptor activity.

To overcome these problems, the electrical monitoring methods of receptor activity have been widely studied. When ligands bind to their specific receptors, biological signals occur. The biological signals can be converted into electrical signals by a transducer [8]. Some processors allow one to measure electrical signals such as conductance changes (Figure 1-1). Further, extensive efforts have been made to develop bioelectronic sensors using biological recognition elements such as receptors [9]. For example, many bioelectronic

sensors using conventional carbon nanotube field effect transistors (CNT-FETs) as a transducer have been developed to monitor receptor activity [9-10].

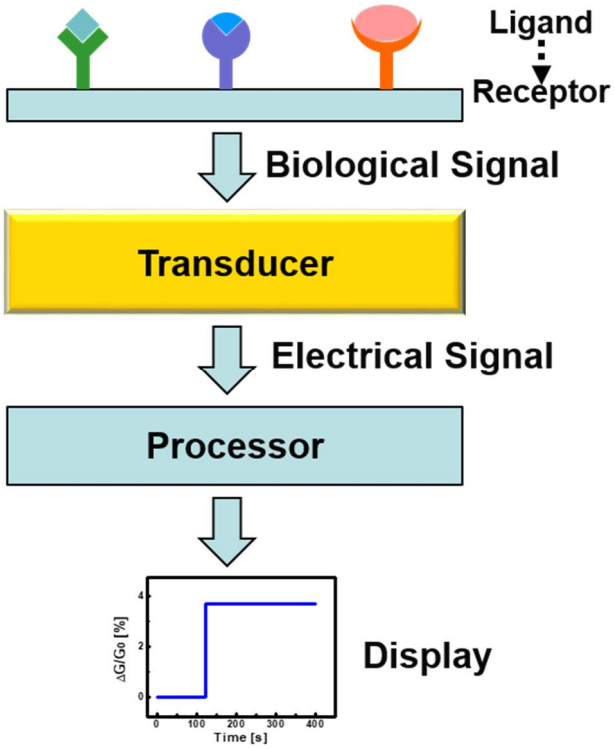

Figure 1-1 Schematic diagram depicting the electrical monitoring of binding signals between receptors and ligands. When ligands bind to their specific receptors, biological signals are generated. The biological signals can be converted into electrical signals through a transducer. One can monitor electrical signals such as conductance changes after some processing.

1.3 Floating Electrode-based Carbon Nanotube Field Effect Transistor

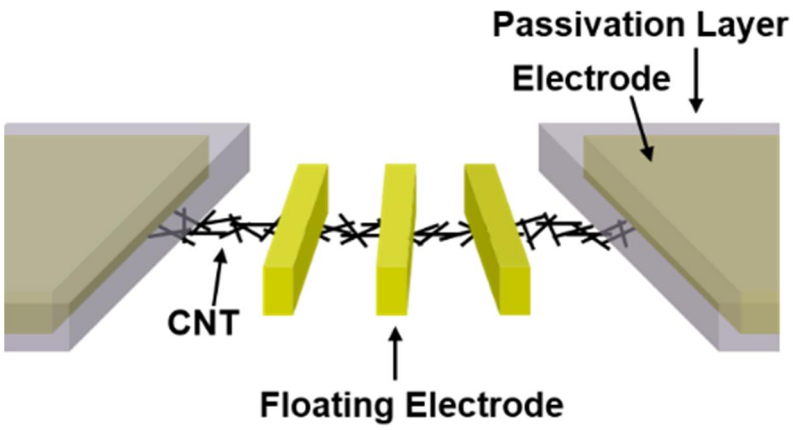

Figure 1-2 Schematic diagram representing a floating electrode-based CNT-FET. CNTs were selectively assembled onto a SiO_2 substrate. Source, drain, and floating electrodes were fabricated via photolithography and thermal deposition. Lastly, a passivation layer was formed onto the source and drain electrodes.

The performance of a bioelectronic sensor depends on the performance of a transducer, because sensor sensitivity and selectivity are mainly determined by a transducer. Previously, the introduction of a floating electrode structure to a conventional CNT-FET was reported (Figure 1-2). A CNT-FET with floating electrodes exhibited enhanced performance than a conventional CNT-FET [11]. When a floating electrode structure is introduced to biological sensors and the binding events of specific target molecules occur on the floating electrodes,

increasing the number of floating electrodes could lead to increased binding events, which results in enhanced sensor sensitivity [12,13]. In addition, a gold (Au)-based floating electrode enables the easy and reliable functionalization of biomolecules on a gold surface. However, previous bioelectronic sensors have relied on a conventional CNT-FET, and a floating electrode structure has not been employed for bioelectronic sensors [14,15]. Thus, bioelectronic sensors based on CNT-FETs with floating electrodes can be simple but powerful tools and are expected to open up a way to study sensory systems for various practical applications.

1.4 References

[1] Grecco, H. E.; Schmick, M.; Bastiaens, P. I. H. *Cell* **2011,** *144*, 897-909.

[2] Rosenbaum, D. M.; Rasmussen, S. G.; Kobilka, B. K. *Nature* **2009,** *459*, 356-363.

[3] Kang, N.; Koo, J. *BMB Rep.* **2012,** *45*, 612-622.

[4] Jacoby, E.; Bouhelal, R.; Gerspacher, M.; Seuwen, K. *ChemMedChem* **2006,** *1*, 761-782.

[5] Absalom, N. L.; Lewis, T. M.; Schofield, P. R. *Exp. Physiol.* **2004,** *89*, 145-153.

[6] Su, J. L.; Fornwald, J.; Rivers, P.; Goldsworthy, S.; Looney, N. A.; Hanvey, J.; Plumpton, C.; Parham, J.; Romanos, M.; Kost, T. A.; Kull, F. C. *J. Immunol. Methods* **2004,** *291*, 123-135.

[7] Zhuang, H.; Matsunami, H. *Nat. Protoc.* **2008,** *3*, 1402-1413.

[8] Perumal, V.; Hashim, U. *J. Appl. Biomed.* **2014,** *12*, 1-15.

[9] Dung, T. T.; Oh, Y.; Choi, S. J.; Kim, I. D.; Oh, M. K.; Kim, M. *Sensors* **2018,** *18*, 103.

[10] Kim, T. H.; Lee, S. H.; Lee, J.; Song, H. S.; Oh, E. H.; Park, T. H.; Hong, S. *Adv. Mater.* **2009,** *21*, 91-94.

[11] Lee, J.; Lee, H.; Kim, T.; Jin, H. J.; Shin, J.; Shin, Y.; Park, S.; Khang, Y.; Hong, S. *Nanotechnology* **2012,** *23*, 085204.

[12] Kim, B.; Lee, J.; Namgung, S.; Kim, J.; Park, J. Y.; Lee, M. S.;

Hong, S. *Sens. Actuators, B* **2012,** *169*, 182-187.

[13] Ta, V. T.; Park, J.; Park, E. J.; Hong, S. *ACS Nano* **2014,** *8*, 2206-2213.

[14] Song, H. S.; Jin, H. J.; Ahn, S. R.; Kim, D.; Lee, S. H.; Kim, U. K.; Simons, C. T.; Hong, S.; Park, T. H. *ACS Nano* **2014,** *8*, 9781-9789.

[15] Jin, H. J.; Lee, S. H.; Kim, T. H.; Park, J.; Song, H. S.; Park, T. H.; Hong, S. *Biosens. Bioelectron.* **2012,** *35*, 335-341.

Chapter 2

Bioelectronic Tongue based on Nanovesicles for the Monitoring of Honeybee Gustatory Receptor Activity to Umami Taste

2.1 Introduction

The sense of taste is closely associated with a human life, because it provides important information about food quality, such as nutritious rich substrates promoting feeding and harmful substrates inhibiting feeding [1,2]. In human and some animal species, sweet, sour, salty, and bitter tastes play an important role in discriminating basic taste qualities. Besides basic taste senses, umami taste, which represents the taste sense of amino acids such as glutamate and 5'-ribonucleotides including inosinate and guanylate, was first recognized as a basic taste sense in 1908 [3]. L-monosodium glutamate (MSG) and 5'-ribonucleotides are known to elicit the umami taste via umami receptors in human and mammals [4]. These taste components are important for food palatability and acceptance in humans. These are widely present in meat, fish, and mushrooms as well as other food products. Additionally, a low concentration of MSG could reduce salt added to foods. However, the unbalance of glutamate levels could cause several disorders such as Alzheimer's diseases [5-8]. Thus, it can be very important to detect excessive MSG in food.

A honeybee, which has been a central insect research model for the study of chemosensory perception [9] and learning and memory [10] can detect a repertoire of taste qualities similar to humans [11].

Although a honeybee genome project has revealed 10 gustatory receptor genes [12], ligands for these gustatory receptors have not yet been identified experimentally. Recently, gustatory receptor 1 of *Apis mellifera* (AmGr1) was identified as a sugar receptor in the honeybee [13] and gustatory receptor 10 of *Apis mellifera* (AmGr10) was specifically tuned to small sets of L-amino acids including umami tastants such as glutamic acid and aspartic acid (unpublished data). Here, we employed a floating electrode-based bioelectronic sensor to utilize the chemosensory function of AmGr10, and find out that AmGr10 could respond to umami substances selectively.

The most noticeable feature of the umami taste is a synergism between MSG and 5'-ribonucleotides such as disodium 5'-inosinate (IMP). 5'-ribonucleotides are well-known as the enhancers of umami taste [14]. This indicates that 5'-ribonucleotides decrease the threshold of sensitivity to MSG and thus increase the sensitivity to the umami taste [4,15]. Recently, there has been a large amount of research on the development of various MSG sensors based on nanomaterials [6,16]. However, these methods intermittently suffered from several limitations. For instance, previous research using carbon nanotubes functionalized with glutamate oxidase can only be employed to detect glutamate-based umami tastants such as MSG [16]. Taken together,

these conventional methods have limitations to characterize the synergism that is the hallmark of the umami taste.

Technically, the performance of sensor transducers is a critical issue in bioelectronic sensors, because it significantly affects device sensitivity and selectivity. Previously, it has been reported that the combination of a floating electrode structure and a carbon nanotube field-effect transistor (CNT-FET) exhibited an enhanced performance as a sensor transducer compared with conventional CNT-FETs [17]. However, floating electrode structures have not been employed for bioelectronic sensor applications, and previous works in this field have relied on simple FET structures [18,19].

In this dissertation, we developed a floating electrode-based bioelectronic tongue mimicking insect taste systems for the discrimination of umami taste substances. In this work, nanovesicles containing honeybee umami taste receptor, AmGr10, were immobilized on a floating electrode-based carbon nanotube sensor transducer to serve as a bioelectronic tongue device for the detection of specific umami tastants. This sensor could discriminate MSG, well-known umami tastant, from non-umami substances with high sensitivity and selectivity. We could also detect umami tastants directly in liquid food such as chicken stock. Significantly, we could quantitatively evaluate

the synergistic effects of IMP to enhance the detection of MSG using a floating electrode-based carbon nanotube sensor incorporated with nanovesicles containing AmGr10. Since this method relies on receptor molecules instead of enzyme, it can be utilized to detect a broad range of umami tastants without being limited to glutamate-based ones. Furthermore, the floating electrode-based devices allow one to improve the sensitivity of previous CNT-based sensors. Our method can be an effective strategy as an artificial taste sensor and thus provides the broad opportunities for basic research on taste sensory systems of animals towards various practical applications in food and other related industries.

2.2 Fabrication of a Floating Electrode-based Bioelectronic Tongue Mimicking Insect Taste System

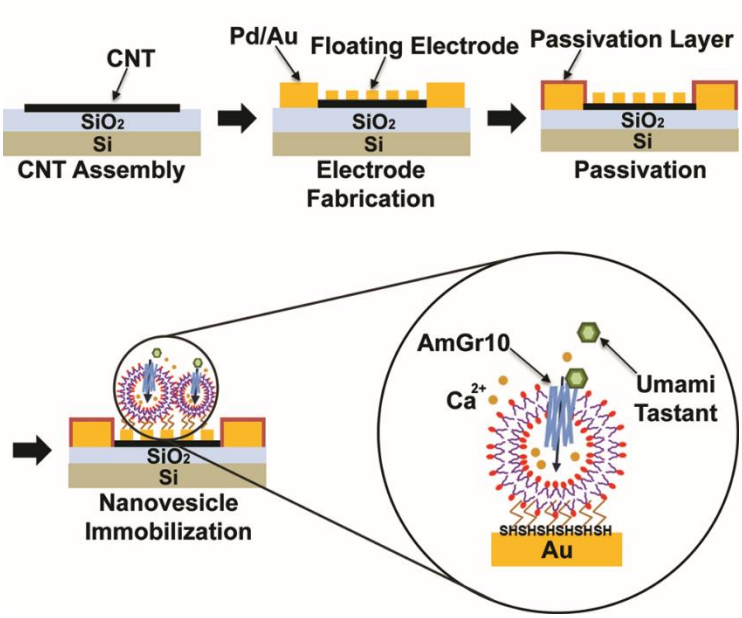

Figure 2-1 Schematic diagram depicting the fabrication process of a floating electrode-based bioelectronic tongue mimicking insect taste systems. A CNT-FET with floating electrodes was hybridized with nanovesicles containing honeybee umami taste receptor, AmGr10. The CNT-FET with floating electrodes was fabricated by photolithography processes. The nanovesicles containing AmGr10 functionalized with thiol groups were immobilized on the gold floating electrodes. AmGr10 can respond to specific umami tastants with high selectivity.

Figure 2-1 is a schematic diagram describing a floating electrode-based carbon nanotube sensor transducer hybridized with nanovesicles containing an umami taste receptor of western honeybees, AmGr10.

First, we fabricated a CNT-FET with floating electrodes as described previously [20-23]. Briefly, CNTs were selectively adsorbed on a SiO_2 substrate, followed by the fabrication of metal electrodes by thermal deposition. Finally, source and drain electrodes were covered by a passivation layer. It has been reported that a biosensor based on a CNT-FET with floating electrodes exhibited higher sensor signals than a conventional biosensor based on a simple CNT-FET [23]. Following the fabrication of the CNT-FET with floating electrodes, we immobilized nanovesicles containing AmGr10 on the floating electrodes of the device. The AmGr10, umami taste receptor, could recognize specific umami tastants. Our fabrication method allows us to mass-produce devices in a wafer scale. In this work, we could fabricate 24 devices on a single wafer and performed sensing experiments using four or more devices for each data point to confirm the reliability of our method.

2.3 Charaterization of AmGr10 in HEK-293T Cells and Nanovesicles

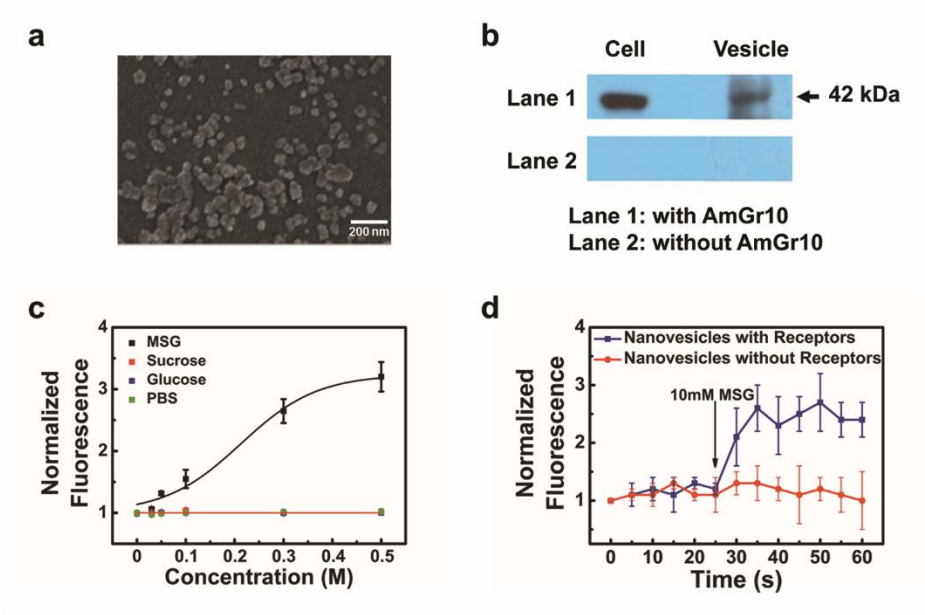

Figure 2-2 Expression of AmGr10 in HEK-293T cells and nanovesicles. (a) FE-SEM image of nanovesicles containing AmGr10 on a gold substrate. (b) Western blot analysis of AmGr10 protein expression in HEK-293T cells and cell-derived nanovesicles. We have obtained rat antiserum against a synthetic peptide from the sequence of AmGr10. Transfected cells and nanovesicles with AmGr10 exhibited the specific band corresponding to the molecular weight of AmGr10, while control cells and nanovesicles (without AmGr10) did not show the band. (c) Dose-dependent intracellular Ca^{2+} assay in HEK-293T cells expressing AmGr10 upon the addition of MSG. Only the addition of MSG caused Ca^{2+} influx in the HEK-293T cells. Each point represents the mean ± SEM of at least ten assays. One-way ANOVA test followed by Bonferroni correction for multiple comparison was employed to test the difference in dose-dependent responses of MSG ($p<0.001$), while Student's t-test was used to test the different responses between MSG and other

substances ($p<0.001$). (d) Real-time measurement of Ca^{2+} assay in the nanovesicles containing AmGr10. The addition of 10 mM of MSG resulted in the increase of fluorescence intensity compared with control nanovesicles without receptors. Each point represents mean ± SEM (Student's t-test: $p<0.05$, N=10).

Figure 2-2a is the field emission scanning electron microscopy (FE-SEM) image of nanovesicles immobilized on a gold surface. Before the SEM imaging, the nanovesicles were lyophilized to maintain their structures and then coated with 10 nm thick platinum using a sputter coater. This image shows that the nanovesicles could be immobilized uniformly on solid surfaces.

Figure 2-2b shows Western blot analysis for the confirmation of AmGr10 expression. In brief, the expressions of AmGr10 protein in HEK-293T cells and cell-derived nanovesicles were confirmed from the lysates of transfected with HEK-293T cells and nanovesicles by Western blot analysis. The AmGr10 antibody is polyclonal and was obtained from rats exposed to a synthetic peptide from the AmGr10 sequence. Lane 1 represents the data from AmGr10-expressing cells and nanovesicles derived from them, while lane 2 represents the data from control cells and nanovesicles. The band of 42 kDa which shows the molecular weight of AmGr10 was observed from the AmGr10-

expressing cells and cell-derived nanovesicles, while the band was not observed from control cells and nanovesicles. These data indicate that AmGr10, the umami taste receptor of the honeybees, was expressed in HEK-293T cells and nanovesicles. In this manner, we determined that the cell derived-nanovesicles contained a sufficient amount of the umami taste receptor of the honeybees. To investigate the functional activity of AmGr10, we carried out the measurement of intracellular calcium concentration changes in AmGr10-expressing HEK-293T cells upon the stimulation of the umami tastant, MSG.

Figure 2-2c shows the dose-dependent intracellular Ca^{2+} assay using Fluo-4 in HEK-293T cells expressing AmGr10. The Ca^{2+} responses were measured by calcium indicator Fluo-4 using a spectrofluorophotometer. The AmGr10-expressing HEK-293T cells exhibited Ca^{2+} responses to MSG above the threshold concentration of 30 mM in a dose-dependent manner. However, intracellular signal transduction did not occur by sweeteners in transfected cells with AmGr10. These results clearly show that AmGr10 was well expressed in the cells, and it selectively responded to umami tastants such as MSG.

We also performed calcium image analysis to identify whether AmGr10-mediated Ca^{2+} influx could activate calcium signals in

nanovesicles. Figure 2-2d shows the real-time measurement of Ca^{2+} assay in nanovesicles containing AmGr10. Note that treatment of the nanovesicles containing AmGr10 with MSG (10 mM) resulted in the immediate increase of fluorescence ratio compared to control nanovesicles without AmGr10. It indicates that the binding of MSG onto the AmGr10 induced a Ca^{2+} influx into the nanovesicles. These data suggested that functional AmGr10 was expressed and incorporated into a cell's plasma membrane, and retained its functional response to agonist when isolated in nanovesicles. In this case, the recovery of calcium signaling to a baseline in the nanovesicles was not observed, probably because of the lack of ion pumps and calmodulin which are necessary to restore the Ca^{2+} concentration [19,24].

2.4 Responses of Bioelectronic Tongues to Umami Taste

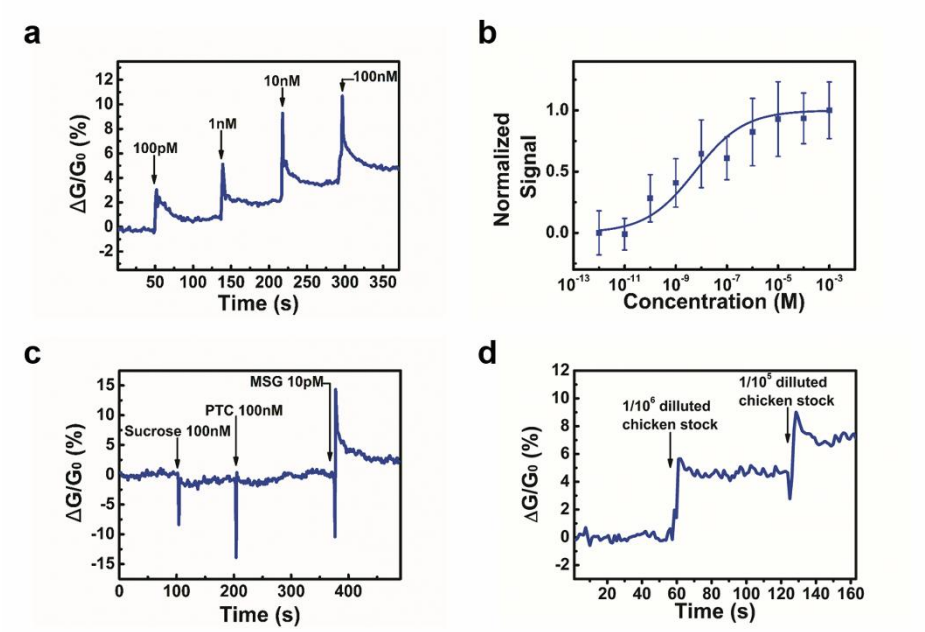

Figure 2-3 Detection of MSG with floating electrode-based bioelectronic tongues. (a) Real-time electrical measurement of MSG. The introduction of MSG caused an increase in the FET channel conductance. The FET channel conductance began to increase after the addition of MSG with 100 pM. (b) Dose-dependent responses of floating electrode-based bioelectronic tongues to MSG. The normalized signal increased as the concentration of MSG increased, and it was saturated at around 10 μM of MSG. We repeated sensing measurements for four or more bioelectronic tongue devices to confirm reliability. The error bars represent the standard deviations of the normalized sensor signals. (c) Real-time response of a floating electrode-based bioelectronic tongue to various tastants. The non-umami tastants (sucrose and PTC) caused negligible FET channel conductance changes, while the introduction of MSG resulted in a large increase in FET channel conductance. (d) Real-time response of a floating electrode-based bioelectronic tongue to

commercial chicken stock solutions diluted with DPBS solutions by $1/10^6$ and $1/10^5$ times from as-purchased commercial chicken stock.

Figure 2-3a shows the real-time response to various concentrations of MSG obtained by a floating electrode-based bioelectronic tongue. A bias voltage of 0.1 V was applied and maintained during electrical measurements. Here, source-drain currents were monitored after the introduction of MSG solutions to the device. As shown in Figure 2-3a, the introduction of MSG solutions resulted in the increase of FET channel conductance with a dose-dependent manner. Here, the sensor signal ($\left|{\Delta G}/{G_0}\right|$) represents relative FET channel conductance change at a certain concentration. Our sensor began to respond to MSG at a concentration of 100 pM, indicating that the floating electrode-based bioelectronic tongue could respond to MSG in real time with high sensitivity. The binding of MSG onto the AmGr10 induced a Ca^{2+} influx into the nanovesicles. Subsequently, the increased concentration of Ca^{2+} in nanovesicles resulted in the increase of the FET channel conductance via the modulation of the Schottky barrier between the CNT networks and the floating electrodes [23]. Note that the conductance increased immediately after the introduction of MSG solutions and then reached stable states. A plausible explanation is that

the concentration of target molecules determines the opening of calcium ion channels in nanovesicles. The binding of target molecules induces a Ca^{2+} influx into nanovesicles, and small nanovesicles can be full of calcium ions and easily reach equilibrium states.

Figure 2-3b shows the normalized signals of floating electrode-based bioelectronic tongues at various concentrations of MSG. The normalized signals of floating electrode-based bioelectronic tongues to each tastant were obtained through normalizing sensor signals with respect to their maximum signal values at high concentrations [18]. We repeated the sensing measurements for four or more bioelectronic tongue devices to calculate averaged values and standard deviations. Even though we use devices fabricated in same condition, there is a little bit of a difference in device characteristics, which led to the variation in responses. Rather narrow error bars indicate that we could obtain reproducible and reliable responses from our floating electrode-based bioelectronic tongues. At a 100 pM or higher concentrations, the sensors exhibited normalized signals larger than error bars, indicating that our sensor can detect MSG down to 100 pM.

The normalized signal increased as the concentration of MSG increased, and it was saturated at a high concentration of 10 μM. Here, the dose-dependent responses of the floating electrode-based

bioelectronic tongues can be analyzed by a model based on a Hill equation as reported previously [18,19,25,26]. First, we assume that binding events between receptors (AmGr10) and MSG follow the Hill equation. Then, the density C_s of MSG bound to the receptors can be written as

(1) $$C_s = \frac{C_{s\,max} \cdot C^n}{(1/K)^n + C^n}$$

Here, C and K are the concentration of MSG in a solution and an equilibrium constant between the AmGr10 and MSG, respectively. $C_{s\,max}$ is the density of AmGr10 on floating electrodes, and n is the value of a Hill coefficient. If we assume that a conductance change ΔG is linearly proportional to the number of bound MSG, the sensor signal $\left|\Delta G/G_0\right|$ can be approximated as $\left|\Delta G/G_0\right| \sim kC_s$, where k is a constant representing the response characteristics of a floating electrode-based bioelectronic tongue. When C becomes very large, the sensor signal $\left|\Delta G/G_0\right|$ converges to the value of $kC_{s\,max}$. Then, we could write the normalized signal N as follows:

(2) $$N = \frac{C^n}{(1/K)^n + C^n}$$

By fitting the experimental data using Eq 2, we can estimate the equilibrium constant K between AmGr10 and MSG as 1.77 x 10^8 M^{-1}.

This quantitative analysis also helps us to predict the responses of our floating electrode-based bioelectronic tongues with the umami taste receptor of the honeybees to its ligand.

Figure 2-3c shows the real-time response of the floating electrode-based bioelectronic tongue to various tastants. Sucrose and phenylthiocarbamide (PTC) are sweet and bitter taste compounds, respectively. The injections of sucrose and PTC with high concentrations of 100 nM caused negligible conductance changes, while that of low concentration MSG caused a sharp increase in the FET channel conductance. This result implies that the floating electrode-based bioelectronic tongue discriminates umami tastants from non-umami tastants with high selectivity.

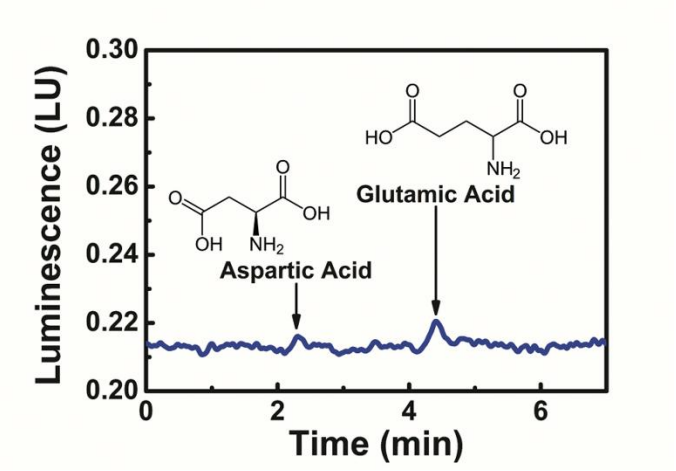

Figure 2-4 HPLC profiles of amino acids in a chicken stock sample. Peaks (black arrows) represent aspartate (Retention Time: 2.30) and glutamate (Retention time: 4.41). The concentration of glutamic acid in the chicken stock sample (1% v/v, in DPBS solution) was 7.1 x 10^{-6} M.

To demonstrate the capability of a floating electrode-based bioelectronic tongue for practical applications, we also performed experiments to detect MSG in a food sample, commercial chicken stock (Figure 2-3d). In brief, the concentration of glutamic acid in the commercial chicken stock was first measured via a high performance liquid chromatography (HPLC) method (Figure 2-4) [27], and the chicken stock was mixed with Dulbecco's Phosphate Buffered Saline (DPBS) solutions with different ratios to prepare watery chicken stock solutions. Based on the HPLC measurement results, the concentrations of glutamic acids in chicken stock solutions diluted by $1/10^6$ and $1/10^5$ times could be estimated as 7.1 x 10^{-10} M and 7.1 x 10^{-9} M, respectively. Then, the diluted chicken stock solutions were applied to a bioelectronic tongue while monitoring its responses. The addition of the chicken stock solution caused significant increases in the FET channel conductance, which shows that our floating electrode-based bioelectronic tongues can detect umami tastants in liquid foods. By fitting the sensor responses via the Hill equation obtained from the data

in clean DPBS solution environments (Figure 2-3b), we could estimate the glutamic acid concentrations of 6.2 x 10^{-10} M and 4.9 x 10^{-9} M in the chicken stock after the addition of $1/10^6$ and $1/10^5$ times diluted chicken stock solutions, respectively. These values are close to the glutamic acid concentrations estimated by the HPLC method within the error bars in Figure 2-3b. These results clearly show that the floating electrode-based bioelectronic tongue can detect MSG in complicated environments such as chicken stock as well as DPBS solution and it can be utilized as a sensor platform for practical applications.

2.5 Quantitative Demonstration of Synergism between L-Monosodium Glutamate (MSG) and 5'-Inosinate (IMP)

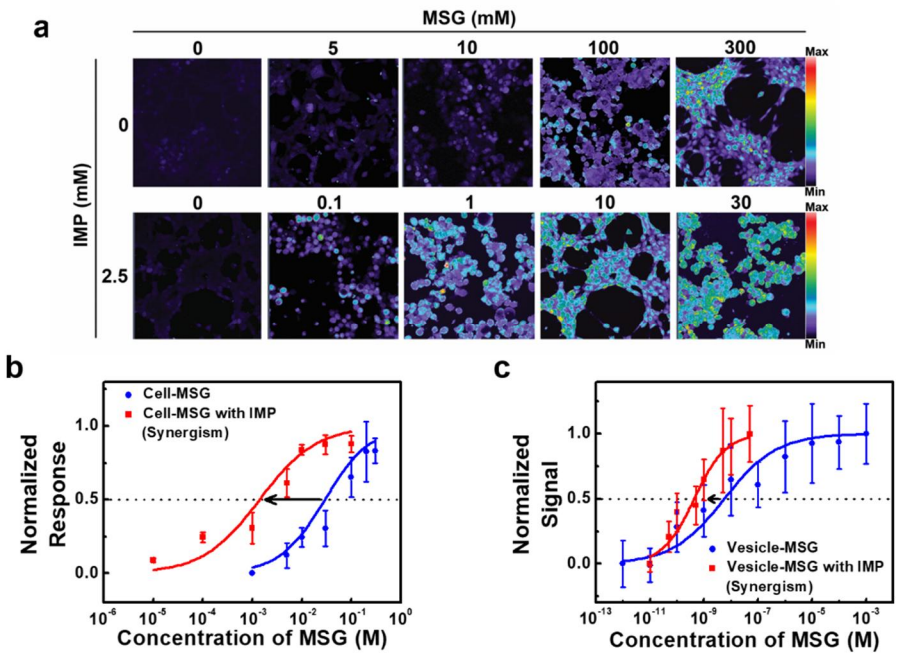

Figure 2-5 Synergism between MSG and IMP in HEK-293T cells and cell-derived nanovesicles. (a) Ca^{2+} fluorescence assay showing dose-responses of AmGr10 to MSG and IMP in HEK-293T cells. The HEK-293T cells expressing AmGr10 were stimulated by MSG with and without IMP (2.5 mM). The results indicated that AmGr10 was activated by MSG and the responses were enhanced by IMP. (b) Dose-response curves of AmGr10 in HEK-293T cells to MSG and MSG with IMP based on the quantitative analysis of Ca^{2+} imaging. We repeated the experiments with nine or more cell samples for quantitative analysis. The error bars represent the standard deviations of the normalized responses. The curves were fitted to the Hill equation. The EC_{50} value of AmGr10 to MSG was shifted 45-fold in the presence 2.5 mM IMP. Values depict the mean ± SEM. (c) Normalized signals of floating electrode-

based bioelectronic tongues with nanovesicles in the presence and absence of 2.5 nM IMP. We repeated sensing measurements for four or more bioelectronic tongue devices to confirm reliability. The error bars represent the standard deviations of the normalized sensor signals. By fitting the curves using the Hill equation, we estimated equilibrium constant K between AmGr10 and MSG as 1.77 x 10^8 M^{-1} and equilibrium constant K_s by synergism between MSG and IMP as 2.30 x 10^9 M^{-1}, respectively. The result showed that the responses to MSG could be enhanced by the synergism between MSG and IMP.

Furthermore, we investigated synergistic effects of disodium 5'-inosinate (IMP), which is known as an enhancer of umami taste, on detecting umami tastants (MSG). This characteristic is a distinctive feature of umami taste sensory systems [1,28,29]. Figure 2-5a shows Ca^{2+} fluorescence assay images showing the dose-dependent responses of AmGr10 in HEK-293T cells to MSG alone and the mixture of MSG and IMP. To examine the effect of IMP, HEK-293T cells expressing AmGr10 were stimulated with various concentrations of MSG in the presence and absence of 2.5 mM (98 mg/100 g) IMP. Previous reports show that IMP can exist in foods with its concentration ranging from 0 to 474 mg/100 g and can give a synergistic effect [30-33]. Our results show that HEK-293T cells expressing AmGr10 responded to MSG at a concentration of 100 mM in the absence of IMP. In contrast, in the

presence of 2.5 mM IMP, the responses of HEK-293T cells expressing AmGr10 to MSG presented much higher fluorescent intensities than the responses in the absence of IMP. Additionally, IMP alone did not activate AmGr10. This result indicates that the response to umami tastant can be strongly enhanced by IMP. This result allows us to verify the synergism, the hallmark of umami taste systems.

Figure 2-5b shows dose-response curves of AmGr10 to MSG in the presence and absence of 2.5 mM IMP based on quantitative analysis of Ca^{2+} imaging in Figure 2-4a. We repeated the experiments with nine or more cell samples for quantitative analysis. The experimental data obtained from Figure 2-4a were fitted by the Hill equation to evaluate equilibrium constants. Here, we could estimate K which is an equilibrium constant between AmGr10 and MSG as 3.45 x 10 M^{-1}. Likewise, an equilibrium constant K_s by the synergism between MSG and IMP can be estimated as 7.14 x 10^2 M^{-1}. These equilibrium constants can be converted to EC_{50} values. The evaluated EC_{50} values are 78.76 mM and 1.73 mM, respectively. This result shows that the EC_{50} value of AmGr10 to MSG was shifted 45-fold in the presence 2.5 mM IMP. This result implies that the responses of AmGr10 to MSG were strongly potentiated by concentrations of IMP comparable to what is found in some foods. Previous studies have

shown the molecular mechanism of synergistic effects of IMP using site-directed mutagenesis and molecular modeling. Human umami taste receptors, T1R1 and T1R3, possess extracellular Venus flytrap domain (VFTD) that consists of two lobes [14]. L-Glutamate binding site of T1R1/T1R3 lies a hinge region of VFTD of T1R1 and IMP binds to an adjacent site close to the opening region of the VFTD of T1R1 [14,34]. Therefore, IMP may act in the extracellular domain of AmGr10 in a similar manner and can strongly potentiate the umami taste intensity as an enhancer in insect taste systems.

We also examined the synergism by utilizing floating electrode-based bioelectronic tongues. Figure 2-5c shows the normalized signals of our platform in the presence and absence of 2.5 nM IMP. Here, the sensing measurements were repeated using four or more bioelectronic tongue devices to confirm reliability. Overall, the bioelectronic tongues responded to the MSG at much lower concentrations than in the case of cell-based assay in Figure 2-4b. Previous works show that nanovesicles responded to analyte solutions with much lower concentrations than cells [19,35,36]. Such results were attributed to the small volume of nanovesicles compared with cells. For example, as the radius R of a vesicle decreases, the volume ($\sim R^3$) decreases much faster than the surface area ($\sim R^2$). Note that the

number of ion channels on the vesicle surface should depend on the surface area of the vesicle. In this case, as the vesicle size decreases, its volume should decrease much faster than the number of ion channels. Thus, relatively small nanovesicles can be filled up more easily by calcium ions, and they respond to lower concentration analytes than cells with a rather large volume [36]. To verify the synergism, we prepared the mixture of MSG and IMP according to the procedure described previously [33]. In the mixture, the concentration of IMP was fixed at 2.5 nM, and that of MSG varied from 10^{-11} M to 5 x 10^{-8} M. As shown in Figure 2-4c, the response curve to MSG was shifted toward lower concentrations. We could also analyze the experimental data by using the model based on the Hill equation. The equilibrium constant K between AmGr10 and MSG can be estimated as 1.77 x 10^{8} M^{-1} in Figure 2-3b. We could estimate K_S which is an equilibrium constant by the synergism between MSG and IMP as 2.30 x 10^{9} M^{-1} in the same way. This result shows that the response of AmGr10 to MSG was significantly enhanced by the synergism between MSG and IMP. That is, the synergistic effects of IMP decrease the threshold of AmGr10 response to MSG. These results show that we could quantitatively evaluate the synergism which is the hallmark of umami taste using floating electrode-based bioelectronic tongues.

2.6 Summary

In summary, we have successfully developed a floating electrode-based bioelectronic tongue mimicking insect taste systems for the discrimination of umami taste substances using the hybridization of floating electrode-based CNT-FETs and nanovesicles containing honeybee umami taste receptor, AmGr10. This bioelectronic tongue recognizes MSG down to 100 pM and discriminates between umami and non-umami substances with high sensitivity and selectivity. The bioelectronic tongue also perceives the presence of MSG in liquid foods such as chicken stock. Importantly, we have demonstrated the synergism between MSG and IMP. Our strategy overcomes the limitations of previous methods in terms of sensitivity and less restrictive experiment conditions. In light of these, a floating electrode-based bioelectronic tongue mimicking insect taste systems can be a simple, but highly effective strategy in many different basic research areas about sensory systems. Moreover, our research provides opportunities to develop various applications in food industry and to research the insect taste systems.

2.7 References

[1] Nelson, G.; Chandrashekar, J.; Hoon, M. A.; Feng, L. X.; Zhao, G.; Ryba, N. J. P.; Zuker, C. S. *Nature* **2002,** *416*, 199-202.

[2] Yarmolinsky, D. A.; Zuker, C. S.; Ryba, N. J. P. *Cell* **2009,** *139*, 234-244.

[3] Nakamura, E. *Chem. - Asian J.* **2011,** *6*, 1659-1663.

[4] Nakashima, K.; Katsukawa, H.; Sasamoto, K.; Ninomiya, Y. *J. Nutr. Sci. Vitaminol.* **2001,** *47*, 161-166.

[5] Barman, S. C.; Hossain, M. F.; Yoon, H.; Park, J. Y. *J. Electrochem. Soc.* **2018,** *165*, B296-B301.

[6] Khan, R.; Gorski, W.; Garcia, C. D. *Electroanalysis* **2011,** *23*, 2357-2363.

[7] Anderson, G. H.; Fabek, H.; Akilen, R.; Chatterjee, D.; Kubant, R. *Appetite* **2018,** *120*, 92-99.

[8] Jinap, S.; Hajeb, P.; Karim, R.; Norliana, S.; Yibadatihan, S.; Abdul-Kadir, R. *Food Nutr. Res.* **2016,** *60*.

[9] Sandoz, J. C. *Front. Syst. Neurosci.* **2011,** *5*, 98.

[10] Giurfa, M.; Sandoz, J. C. *Learn. Mem.* **2012,** *19*, 54-66.

[11] Sanchez, M. G. D. *Chem. Senses* **2011,** *36*, 675-692.

[12] Weinstock, G. M.; Robinson, G. E.; Gibbs, R. A.; Worley, K. C.; Evans, J. D.; Maleszka, R.; Robertson, H. M.; Weaver, D. B.; Beye, M.; Bork, P.; *et al*. *Nature* **2006,** *443*, 931-949.

[13] Jung, J. W.; Park, K. W.; Ahn, Y. J.; Kwon, H. W. *J. Asia-Pac. Entomol.* **2015,** *18*, 19-26.

[14] Zhang, F.; Klebansky, B.; Fine, R. M.; Xu, H.; Pronin, A.; Liu, H. T.; Tachdjian, C.; Li, X. D. *Proc. Natl. Acad. Sci. U. S. A.* **2008,**

105, 20930-20934.

[15] Delay, E. R.; Beaver, A. J.; Wagner, K. A.; Stapleton, J. R.; Harbaugh, J. O.; Catron, K. D.; Roper, S. D. *Chem. Senses* **2000,** *25*, 507-515.

[16] Koh, J.; Yi, M.; Yang Lee, B.; Kim, T. H.; Lee, J.; Jhon, Y. M.; Hong, S. *Nanotechnology* **2008,** *19*, 505502.

[17] Lee, J.; Lee, H.; Kim, T.; Jin, H. J.; Shin, J.; Shin, Y.; Park, S.; Khang, Y.; Hong, S. *Nanotechnology* **2012,** *23*, 085204.

[18] Jin, H. J.; Lee, S. H.; Kim, T. H.; Park, J.; Song, H. S.; Park, T. H.; Hong, S. *Biosens. Bioelectron.* **2012,** *35*, 335-341.

[19] Song, H. S.; Jin, H. J.; Ahn, S. R.; Kim, D.; Lee, S. H.; Kim, U. K.; Simons, C. T.; Hong, S.; Park, T. H. *ACS Nano* **2014,** *8*, 9781-9789.

[20] Lee, M.; Im, J.; Lee, B. Y.; Myung, S.; Kang, J.; Huang, L.; Kwon, Y. K.; Hong, S. *Nat. Nanotechnol.* **2006,** *1*, 66-71.

[21] Park, J.; Lim, J. H.; Jin, H. J.; Namgung, S.; Lee, S. H.; Park, T. H.; Hong, S. *Analyst* **2012,** *137*, 3249-3254.

[22] Kim, T. H.; Lee, S. H.; Lee, J.; Song, H. S.; Oh, E. H.; Park, T. H.; Hong, S. *Adv. Mater.* **2009,** *21*, 91-94.

[23] Kim, B.; Lee, J.; Namgung, S.; Kim, J.; Park, J. Y.; Lee, M. S.; Hong, S. *Sens. Actuators, B* **2012,** *169*, 182-187.

[24] Dong, H.; Dunn, J.; Lytton, J. *Biophys. J.* **2002,** *82*, 1943-1952.

[25] Jin, H. J.; An, J. M.; Park, J.; Moon, S. J.; Hong, S. *Biosens. Bioelectron.* **2013,** *49*, 86-91.

[26] Kim, T. H.; Song, H. S.; Jin, H. J.; Lee, S. H.; Namgung, S.; Kim, U. K.; Park, T. H.; Hong, S. *Lab Chip* **2011,** *11*, 2262-2267.

[27] Van Boven, M.; Daenens, P.; Cokelaere, M.; Decuypere, E. *J.*

Chromatogr. B: Biomed. Sci. Appl. **1994,** *655*, 281-285.

[28] Yoshii, K.; Yokouchi, C.; Kurihara, K. *Brain Res.* **1986,** *367*, 45-51.

[29] Li, X. D.; Staszewski, L.; Xu, H.; Durick, K.; Zoller, M.; Adler, E. *Proc. Natl. Acad. Sci. U. S. A.* **2002,** *99*, 4692-4696.

[30] Fuke, S.; Konosu, S. *Physiol. Behav.* **1991,** *49*, 863-868.

[31] Drake, S. L.; Whetstine, M. E. C.; Drake, M. A.; Courtney, P.; Fligner, K.; Jenkins, J.; Pruitt, C. *J. Food Sci.* **2007,** *72*, S360-S366.

[32] Ninomiya, K. *Food Rev. Int.* **1998,** *14*, 177-211.

[33] Yamaguchi, S. *J. Food Sci.* **1967,** *32*, 473-478.

[34] Cascales, J. J. L.; Costa, S. D. O.; de Groot, B. L.; Walters, D. E. *Biophys. Chem.* **2010,** *152*, 139-144.

[35] Pick, H.; Schmid, E. L.; Tairi, A. P.; Ilegems, E.; Hovius, R.; Vogel, H. *J. Am. Chem. Soc.* **2005,** *127*, 2908-2912.

[36] Christensen, S. M.; Stamou, D. G. *Sensors* **2010,** *10*, 11352-11368.

Chapter 3

Bioelectronic Nose based on Nanodiscs for the Monitoring of Human Olfactory Receptor Activity to a Rose Scent

3.1 Introduction

A rose scent is known to be a pleasant smell to humans, and it has been used as a key component to impart scents to various fragrances and flavorings [1]. Some of the well-known ingredients for a rose scent are geraniol, citronellol, phenylethyl alcohol, nerol, and so on [2-4]. Rose oil products including such ingredients have often been utilized as one of the base materials for developing new perfumes, making the perfumes more complete and plentiful [5,6]. However, the overdose of such rose scent ingredients can cause bad smells and even allergic reactions to humans. Thus, the quantitative evaluation of rose scent ingredients in real samples such as rose oil can be an important issue and has been extensively studied in various areas such as cosmetic and pharmaceutical industries [7,8]. However, most of methods allow one to measure only specific well-known substances, and they cannot be used to measure how humans would respond to some new substances. Furthermore, they often exhibited rather low selectivity compared with a human nose.

In humans and mammals, an olfactory system enables the discrimination of specific chemical components from other non-specific components, which has been critical in evaluating food quality

and recognizing dangers in various environments [9,10]. In an olfactory system, olfactory receptor (OR) proteins recognize and bind only to specific odorant molecules, enabling the identification of specific smells [11]. For example, the main ingredients of a rose scent, geraniol and citronellol, could specifically bind to human olfactory receptor 1A2 (hOR1A2) with different characteristics [5,12,13]. Such selective binding characteristics of ORs have been utilized to develop bioelectronic nose sensors with human-like responses [11,14]. For example, versatile bioelectronic noses have been developed by hybridizing ORs onto electric channels based on various nanostructures such as carbon nanotubes (CNTs), conducting polymer nanotubes, and graphene [15-17]. However, it is often difficult to ensure the structural stability of ORs and to achieve the stable immobilization of ORs on such nanostructured material surfaces, degrading the stability and sensitivity of the bioelectronic nose devices based on them [15,18]. Furthermore, bioelectronic nose devices to detect general rose scent ingredients have not been developed yet.

In this dissertation, we report a strategy for the human-like smelling of rose scent ingredients in real samples using olfactory receptor nanodisc (ND)-based bioelectronic nose devices. In this strategy, hOR1A2 was expressed from *Escherichia coli* (*E. coli*) and

reconstituted using the ND structure. The hOR1A2-embedded nanodiscs (hOR1A2NDs) were successfully incorporated on gold (Au)-based floating electrodes over a CNT-FET. We could monitor the binding of target rose scent molecules onto the NDs via the subjacent CNT-based transistor. This method allowed us to identify and quantitatively monitor geraniol and citronellol, well-known rose odorants, down to 1 fM and 10 fM, respectively. This method can also be used to discriminate a specific rose odorant from other odorants just like a human olfactory system. Furthermore, we utilized our devices to quantitatively evaluate the effect of scent enhancer materials on the responses of ORs and found that when 1 nM benzyl salicylate was added, the ORs responded to rose odorants with ~10^3 times lower concentrations. Importantly, the method enabled the quantitative evaluation of rose odorants in a real sample like rose oil. Since our method allows one to quantitatively evaluate general ingredients providing a rose scent even in real samples, it could be a powerful tool for versatile basic research and industrial applications such as the screening of new rose scent ingredients and the quantitative evaluation of base materials for fragrances.

3.2 Structure of a Bioelectronic Nose Comprised of hOR1A2-embedded Nanodiscs and a Carbon Nanotube-based Transistor with Floating Electrodes

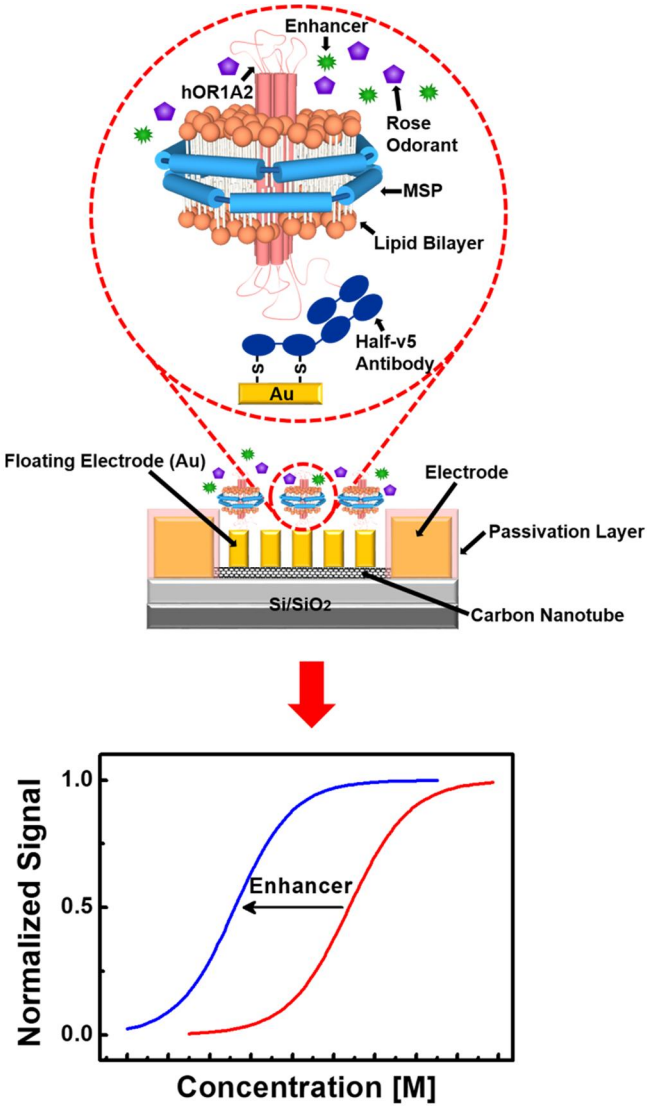

Figure 3-1 Schematic diagram depicting a bioelectronic nose based on the hybridization of hOR1A2-embedded nanodiscs (hOR1A2NDs) and a floating electrode-based CNT-FET, and the simplified sensor responses of a

bioelectronic nose. The hOR1A2NDs were immobilized on the gold-based floating electrodes of the CNT-FET using half-v5 Ab fragments and thiol groups. Bioelectronic noses could specifically respond to general rose scent ingredients just like a human nose.

Figure 3-1 shows a schematic diagram depicting a bioelectronic nose which was fabricated via the hybridization of hOR1A2NDs and a CNT-based transistor with floating electrodes. In brief, hOR1A2 was overexpressed in *E. coli* and purified via affinity chromatography. Then, the purified hOR1A2 proteins were wrapped with lipid bilayers and membrane scaffold proteins (MSPs) for the construction of hOR1A2-based NDs. The prepared hOR1A2NDs were selectively immobilized on the flat gold floating electrodes of the CNT-based transistor. Here, the gold floating electrodes were first functionalized with thiol groups, and then the gold surfaces were functionalized with half-v5 antibody (Ab) fragments via disulfide bonding [19,20]. Subsequently, the hOR1A2NDs were incorporated on the gold-based floating electrodes. Lastly, the CNT-FETs was washed with a HEPES buffer II solution several times to remove unbound hOR1A2NDs. When specific rose odorants bound to the hOR1A2 on the floating electrode, the conductance of the CNT-FET channel was changed, which allowed us to monitor rose scent ingredients in real-time. In this fabrication

strategy, receptor molecules stabilized in ND structures were directly and directionally immobilized on a flat gold-based floating electrode surface using well-known reliable chemical processes, which should simplify the chemical procedures and may enhance the reliability of our devices compared with previous CNT channel-based sensor devices [15,21]. Furthermore, we can take advantage of the high sensitivity of floating electrode-based transducers as reported previously [22]. Finally, since the hOR1A2 molecules bind selectively to general rose odorant molecules like a human nose, we can expect our sensors to smell a rose scent just like humans.

3.3 Characterization of hOR1A2 Expressed in HEK-293 Cells and Nanodiscs

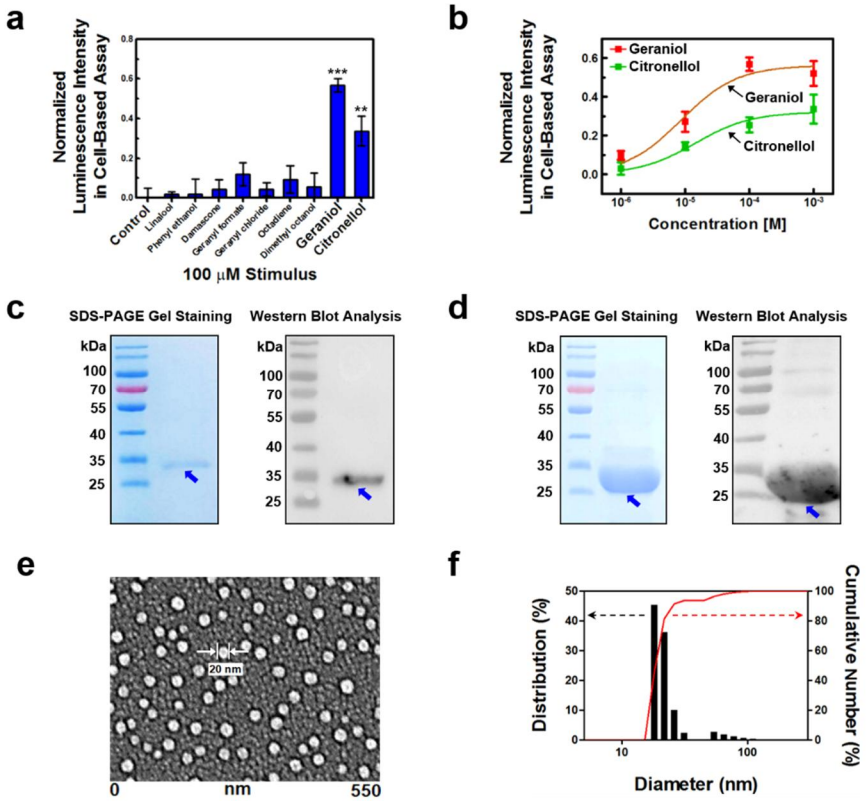

Figure 3-2 Characterization of hOR1A2 expressed in HEK-293 cells and NDs. (a) Specificity of hOR1A2 to geraniol and citronellol among various odorants. Only the stimulation of geraniol and citronellol caused responses in HEK-293 cells with hOR1A2 (**p<0.01, ***p<0.001) (n=5). (b) Dose-dependent responses of hOR1A2 expressed in HEK-293 cells upon the addition of geraniol and citronellol. The HEK-293 cells expressing hOR1A2 exhibited luminescence intensities to geraniol and citronellol with different characteristics (n=5). (c) SDS-PAGE gel staining image and western blot analysis of purified hOR1A2 expressed in *E. coli*. The band of 34 kDa indicates the molecular weight of hOR1A2. (d) SDS-PAGE gel staining image

and western blot analysis of purified MSP1E3D1 expressed in *E. coli*. The band of 26 kDa corresponding to the molecular weight of MSP1E3D1 was observed. (e) FE-SEM image of hOR1A2NDs immobilized on a gold substrate. The NDs were immobilized uniformly on the gold surface, and their diameters ranged from 15 nm to 20 nm. (f) Size distribution analysis of hOR1A2NDs.

We performed cell-based assays to evaluate the ligand/receptor binding activity of hOR1A2 in cells and to compare it with the binding activity of hOR1A2 in our bioelectronic nose devices [23]. Figure 3-2a shows the responses of hOR1A2 in HEK-293 cells to various kinds of odorants with 100 μM concentrations. In brief, hOR1A2 and luciferase gene were first transfected in the HEK-293 cells. When the binding of the specific odorants to hOR1A2 in the transfected cells occurred, the conformation of hOR1A2 was changed and signal transduction was initiated. A cyclic adenosine monophosphate (cAMP) pathway in the cells was sequentially activated. The activated cAMP pathway stimulated cAMP response element-binding protein (CREB), which resulted in the expression of luciferase gene [24]. A luminescence intensity in the cells was measured using a Dual-Glo luciferase assay system after the introduction of different odorants. A normalized luminescence intensity was calculated by normalizing the responses of hOR1A2 to each odorant with respect to a positive control (forskolin,

FSK) in HEK-293 cells. Linalool, phenyl ethanol, and damascone have pleasant floral odors. They are often used to make an artificial rose scent with geraniol and citronellol. Geranyl formate and geranyl chloride have different functional groups from geraniol. Octadiene and dimethyl octanol have different numbers of carbon atoms and carbon-carbon double bonds compared with geraniol, respectively. The HEK-293 cells expressing hOR1A2 stimulated by geraniol and citronellol resulted in much higher luminescence intensities compared to those stimulated by other odorants. These results show that hOR1A2 discriminates the specific rose odorants from other odorants with high selectivity, indicating that hOR1A2 was well expressed and retained its functionality in the cells.

Figure 3-2b displays the dose-dependent responses of hOR1A2-expressing HEK-293 cells to geraniol and citronellol. The responses of hOR1A2 in the HEK-293 cells to different concentrations of geraniol and citronellol were measured by the luciferase assay system in a similar way to that of Figure 3-2a. The response data were fitted using a Hill equation to evaluate dissociation constants (K_d) and Hill coefficients. The HEK-293 cells expressing hOR1A2 exhibited luminescence intensities to geraniol and citronellol from the concentrations of 1 μM and 10 μM, respectively. The dissociation

constants (K_d) of hOR1A2 to geraniol and citronellol were calculated as 3.24×10^{-6} M and 1.45×10^{-5} M, respectively. These constant values are quite similar to those in other studies using mammalian cell-based systems [25,26]. The results imply that functional hOR1A2 was successfully produced in the HEK-293 cells, while maintaining its functionality. Also, we can see that the receptors in the cells exhibited larger responses to geraniol than citronellol, presumably due to the higher affinity of hOR1A2 to geraniol than citronellol. The Hill coefficients were estimated as 0.55 and 0.52 for geraniol and citronellol, respectively. This indicates that the binding of geraniol and citronellol to hOR1A2 could be considered as negatively cooperative bindings [27]. Previous works show that for most GPCRs, the binding of one ligand to one binding site causes the structural change of neighboring binding sites, which may lead to a lower affinity for other ligands like our results [28-30].

For the development of bioelectronic nose devices smelling a rose scent, we expressed hOR1A2 in *E. coli* and performed the extraction and functional reconstruction of hOR1A2 molecules in solution [19,31,32]. Figure 3-2c shows the sodium dodecyl sulfate polyacrylamide gel electrophoresis (SDS-PAGE) gel staining image (left) and western blot analysis (right) of purified hOR1A2 expressed in

E. coli. For the formation of high-quality receptor proteins, hOR1A2 was overexpressed in *E. coli*, solubilized and purified with affinity chromatography. The purification and expression of hOR1A2 in *E. coli* were confirmed by a SDS-PAGE method and western blot analysis. The bands of 34 kDa, which are in accord with the molecular weight of hOR1A2, were clearly observed. These results indicate that hOR1A2 was well produced in *E. coli* and highly purified. It should be pointed out that it has been very difficult to express and purify G protein-coupled receptors (GPCRs) in heterologous cells, especially in *E. coli* due to their complicated structures and hydrophobicity. Such a difficulty has been a stumbling block holding back the practical applications of OR-based biosensor devices [33,34]. Considering that the successful expression of hOR1A2 in *E. coli* has not been reported before, our results can be a breakthrough and could provide more opportunities for biosensors and other applications requiring a large amount of high-quality OR proteins responding to a rose scent.

To achieve a stable OR functionality on our bioelectronic nose devices, hOR1A2 was embedded in ND structures. First, MSP1E3D1, which is MSP derived from apolipoprotein A-I in humans, was produced and purified to wrap lipid/receptor complexes [35]. Figure 3-2d shows the SDS-PAGE gel staining image (left) and western blot

analysis (right) of purified MSP1E3D1. The expression and purification of MSP1E3D1 were confirmed in a similar way to that of Figure 3-2c. The thick bands around 26 kDa were clearly observed. The bands correspond to the molecular weight of MSP1E3D1. These indicate that MSP1E3D1 was overexpressed, successfully produced as a soluble form, and purified with high purity. Because it has been reported that MSP1E3D1 can be overexpressed in *E. coli* and its overexpression allows it to effectively wrap lipid/receptor complexes [36], our results imply that MSP1E3D1 was successfully overexpressed to construct stable ND structures for the development of bioelectronic devices.

To construct hOR1A2-embedded NDs, the purified MSP1E3D1 was added to the mixture of hOR1A2 and lipids. Then, the detergent molecules of the mixture were removed with Bio-beads. The purified hOR1A2NDs were finally obtained by size exclusion chromatography (SEC). Figure 3-2e shows the field emission scanning electron microscopy (FE-SEM) image of hOR1A2NDs incorporated on the surface of a gold. To maintain the structure of hOR1A2NDs, the hOR1A2NDs immobilized on the gold surface were lyophilized using a freeze dryer. Then, the surface was covered with platinum (5 nm) by a sputtering system. The hOR1A2NDs ranged in diameter from 15 nm to 20 nm. This clearly shows that we successfully constructed

hOR1A2NDs with optimized sizes and could immobilize them uniformly on gold surfaces.

To confirm the size distribution of the constructed hOR1A2NDs, we performed a dynamic light scattering (DLS) analysis. Figure 3-2f shows that the hOR1A2NDs had uniform diameters from 15 nm to 20 nm with a quite narrow size distribution, which is similar to that of Figure 3-2e. The size distribution of hOR1A2NDs is also close to that of NDs containing other GPCRs in previous studies [37,38]. This implies that hOR1A2NDs can be successfully constructed as monomeric receptor forms and can be utilized as an ideal sensor unit.

3.4 Electrical Responses of Bioelectronic Noses

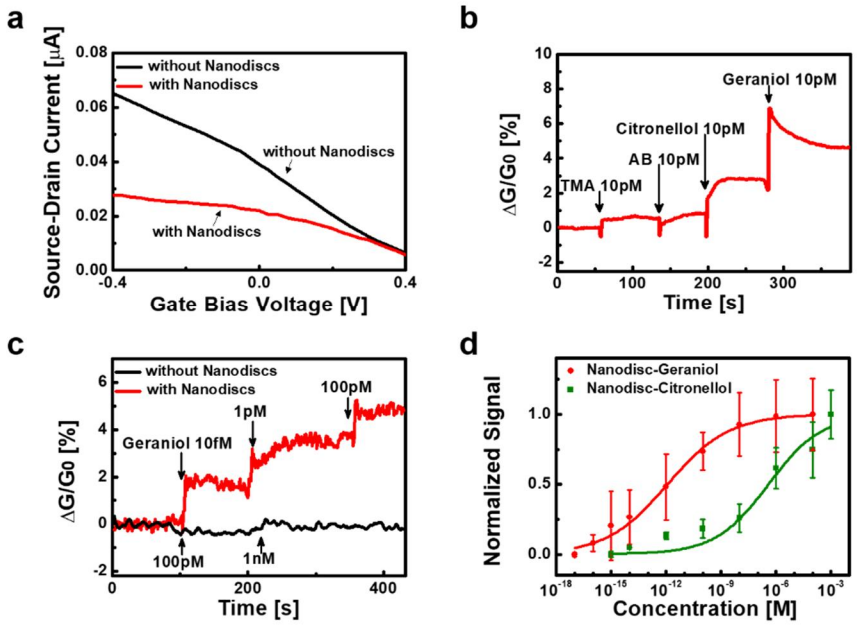

Figure 3-3 Electrical measurement data of ND-based bioelectronic noses. (a) Liquid gate profiles of a CNT-FET with floating electrodes before and after the immobilization of hOR1A2NDs. The CNT-FET with floating electrodes exhibited a typical p-type semiconducting property, and its characteristic was maintained after the immobilization of hOR1A2NDs. (b) Real-time responses of a bioelectronic nose to different kinds of odorants. The addition of geraniol and citronellol of 10 pM concentrations caused significant increases in the CNT-FET channel conductance, while the addition of TMA and AB of 10 pM concentrations resulted in negligible changes in the CNT-FET channel conductance. (c) Real-time responses of a bioelectronic nose device with or without hOR1A2NDs to various concentrations of geraniol. The introduction of geraniol occurred sharp increases in the channel conductance of the bioelectronic nose, while there was no meaningful conductance change in the bare CNT-FET without NDs. (d) Dose-dependent responses of bioelectronic noses to geraniol and citronellol. Each point and error bar represent the

average value and standard deviation of multiple sensing measurements, respectively. Bioelectronic noses began to show responses to geraniol with the concentration of 1 fM, and the responses were almost saturated at around 1 μM. Bioelectronic noses also exhibited the responses from 10 fM concentration of citronellol.

Figure 3-3a shows the liquid gate profiles of a floating electrode-based CNT transistor before and after the immobilization of hOR1A2NDs. Source-drain currents were measured at a gate bias voltage ranging from -0.4 V to 0.4 V with the application of 0.1 V source-drain bias voltage. The source-drain currents decreased significantly as the applied gate voltage increased, indicating the typical p-type semiconducting behavior of the CNT-FET device. Note that the conductance of the CNT-FET channel decreased after the immobilization of hOR1A2NDs, which could be attributed to the negatively charged C-terminuses of the NDs immobilized on the floating electrodes [39]. The negatively-charged NDs reduced the CNT channel conductance, which was attributed to Schottky barrier modulation at the CNT-floating electrode contacts. Also, it should be mentioned that the gating effect of the CNT-FET device was maintained even after the immobilization of hOR1A2NDs, indicating that it can be suitable for sensor applications [40].

Figure 3-3b shows the real-time responses of a bioelectronic nose to various odorants. Trimethylamine (TMA) and amyl butyrate (AB) are odorants generated from spoiled seafood and reminiscent of an apricot, respectively. When the source-drain bias of 0.1 V was applied, source-drain currents were observed during the addition of different odorant solutions. In this sensor device, a relative CNT-FET channel conductance change $\Delta G/G_0$ was used as a sensor signal, where ΔG and G_0 are the conductance change and original conductance of the CNT-FET, respectively. The introduction of geraniol and citronellol solutions of 10 pM concentrations caused significant increases in the conductance of the CNT channel. However, the introduction of TMA and AB with the same concentrations induced negligible changes. This result indicates that our bioelectronic nose could highly selectively discriminate rose scent odorants from other odorants.

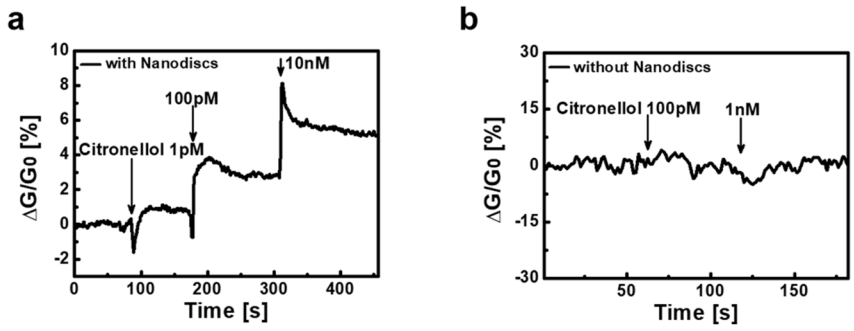

Figure 3-4 Real-time responses of a bioelectronic nose device with or without hOR1A2NDs to various concentrations of citronellol. (a) Real-time responses of a ND-based bioelectronic nose to different concentrations of citronellol. The addition of citronellol resulted in the sharp increases in the CNT-FET channel conductance. (b) Real-time responses of a bare CNT-FET without hOR1A2NDs to various concentrations of citronellol. The bare CNT-FET without hOR1A2NDs did not respond to citronellol.

Figure 3-3c displays the typical real-time responses of a bioelectronic nose with or without hOR1A2NDs to varying concentrations of geraniol in aqueous environments. Source-drain currents were measured during the addition of geraniol solutions with different concentrations. The addition of geraniol solutions caused immediate increases in the conductance of the CNT-FET with hOR1A2NDs in a dose-dependent manner, while the bare CNT-FET without hOR1A2NDs did not exhibited conductance changes even after the addition of geraniol. We could obtain a similar selective response when citronellol was applied to CNT-FET devices with or without hOR1A2NDs (Figure 3-4). The result clearly shows that the sensor responses came from the specific binding between the rose odorants and hOR1A2. Such a specific response can be attributed to the change of electrical charges in the hOR1A2 caused by the selective binding of rose odorant molecules. In brief, the specific binding of rose odorant

molecules to hOR1A2 caused the conformational change of the receptor, resulting in the change of electrical charges in it [14]. Subsequently, the changed charge state of the receptor molecule would result in the increase in the conductance of the CNT channel via Schottky barrier modulation at CNT-floating electrode contacts [22,41]. This result shows that our method can allow us to highly sensitively detect specific rose odorants in real-time.

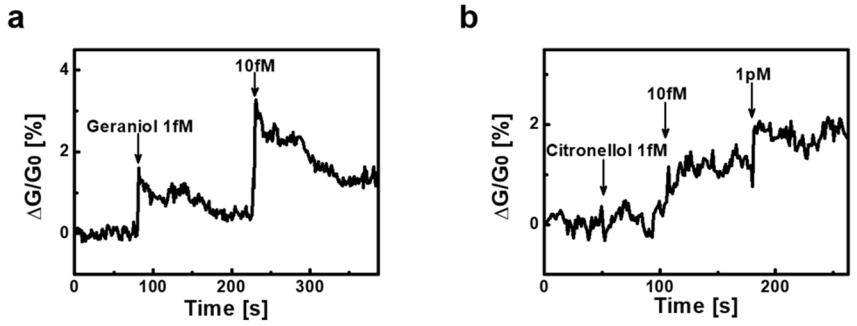

Figure 3-5 Real-time responses of ND-based bioelectronic noses to geraniol and citronellol to confirm reliability. (a) Real-time responses of a ND-based bioelectronic nose to various concentrations of geraniol. The bioelectronic nose began to respond to geraniol at the concentration of 1 fM with a signal-to-noise ratio of ~ 4.4. (b) Real-time responses of a ND-based bioelectronic nose to different concentrations of citronellol. The graph shows that the bioelectronic nose responded to citronellol of 10 fM with a signal-to-noise ratio of ~ 5.5.

Figure 3-3d displays the normalized sensor signals of our

bioelectronic noses to geraniol and citronellol with different concentrations. The normalized signals were calculated by normalizing sensor signals regarding their maximal sensor signal values at high concentration conditions [22,42,43]. The sensing measurement at a single concentration was carried out repeatedly using multiple bioelectronic noses to obtain average values and standard errors. The result shows the response curves similar to those of other bioelectronic nose devices reported previously [18,40]. In the case of geraniol, our bioelectronic noses began to show responses from the concentration of 1 fM (signal-to-noise ratio of ~4.4, Figure 3-5), and the responses were almost saturated around 1 μM. For citronellol, bioelectronic noses exhibited the responses from the concentration of 10 fM (signal-to-noise ratio of ~5.5, Figure 3-5). These results indicate that our bioelectronic noses could detect the rose scent odorants with high sensitivity and discriminate one rose scent odorant from the other odorant. It is worth discussing the effects of possible impurities in the chemicals used in our experiments because, at such a low target concentration, the effect of the impurities on sensor signals may be comparable to that by target molecules. First of all, the impurity content in the target chemicals containing target molecules was less than 5% in our experiments. Furthermore, when the target chemicals were diluted

to lower concentrations, their impurities should also be diluted in the same proportion. Therefore, even though bioelectronic noses were stimulated by target chemicals with a very low concentration, the impurities should not affect sensing signals much. On the other hand, the impurity concentrations in a HEPES buffer solution, which was used as a solvent to prepare target solutions, should have remained identical even in target solutions with a very low target concentration. However, we found that our bioelectronic noses did not respond to the HEPES buffer solution without any target molecules, indicating that the effect by impurities is not significant even in the target solution with a very low target concentration.

The dose-dependent responses of our bioelectronic noses can be analyzed further using a model based on a Hill-Langmuir equation as reported previously [19,22,42,43]. If we suppose that binding characteristics between target odorant molecules (geraniol and citronellol) and receptors (hOR1A2) comply with the model, the surface density C_s of the odorant molecules bound to hOR1A2 in the NDs can be simply written like

(1) $$C_s = \frac{C_{s\_max} \cdot C^n}{(1/K)^n + C^n}$$

C is the *concentration of the applied odorant solution*, and K is an

equilibrium constant for the binding of the odorants to hOR1A2. C_{s_max} denotes the *density of hOR1A2 on the floating electrodes*, and n represents a *Hill coefficient*. Assuming a conductance change ΔG is nearly proportional linearly to the number of adsorbed odorant molecules, the sensor signal $\left|\Delta G/G_0\right|$ could be simplified as $\left|\Delta G/G_0\right| \sim kC_s$. Here, k represents a constant signifying the response characteristics of a bioelectronic nose. The sensor signal $\left|\Delta G/G_0\right|$ converges to the maximum value of kC_{s_max} as C becomes very large. Therefore, a normalized signal N could be written like

$$N = \frac{C^n}{(1/K)^n + C^n} \quad (2)$$

The experimental data were fitted by Eq. (2), and the equilibrium constants of geraniol and citronellol to hOR1A2 were estimated as 8.37 $\times$ 10^{11} M^{-1} and 2.60 $\times$ 10^6 M^{-1}, respectively. Note that the equilibrium constant of geraniol was found ~10^5 times larger than that of citronellol. The results imply that geraniol could be a more potent rose scent than citronellol, which is consistent with the result using cells in Figure 3-2b. However, the results show that our bioelectronic noses responded to much lower concentrations of geraniol and citronellol than the case of the cell-based assays in Figure 3-2b. Presumably, it is because our

device could directly measure the conformation of receptor proteins without any intermediate biological steps, while, the cell assays relied on complicated signal transduction steps based on multiple biological processes caused by the binding of odorant molecules to receptors [44-47]. The intermediate steps in the cell assays require several different materials other than rose odorants to generate the sensing signals, which could have resulted in much lower sensitivity than the bioelectronic noses [33]. Similar trends were also reported in case of other bioelectronic devices [22,42]. The Hill coefficients *n* were estimated as 0.26 and 0.30 for geraniol and citronellol, respectively. This also indicates the negatively cooperative binding of geraniol and citronellol to hOR1A2 on bioelectronic noses [48]. Note that the Hill coefficients in bioelectronic noses were smaller than those in the cell-based assays as shown in Figure 3-2b. Presumably, it is because of the possible aggregation and steric hindrance of receptor proteins on our bioelectronic nose devices [48]. Since our method is based on these bioelectronic noses, it can be a sensitive platform for versatile utilization such as the development of new fragrances.

3.5 Measuring the Effects of a Scent Enhancer on the Assessment of Rose Scent Ingredients

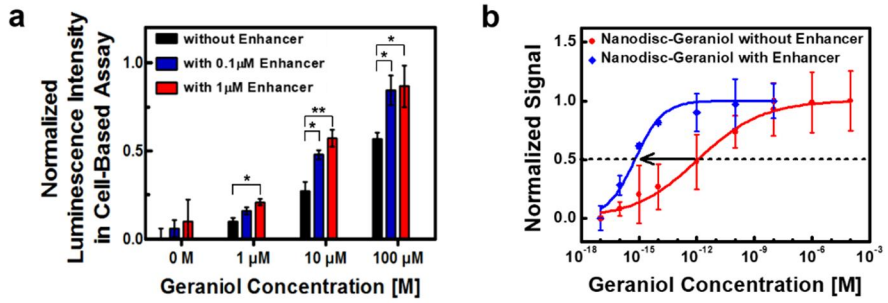

Figure 3-6 Effect of benzyl salicylate as an enhancer on the assessment of geraniol by utilizing hOR1A2-expressing HEK-293 cells and bioelectronic noses. (a) Normalized luminescence intensities of hOR1A2 to geraniol and benzyl salicylate in HEK-293 cells. The HEK-293 cells expressing hOR1A2 were activated by geraniol with or without varying concentrations of benzyl salicylate (0, 0.1, 1 μM). The responses of hOR1A2 to geraniol were enhanced by benzyl salicylate (*$p<0.05$, **$p<0.01$) (n=5). (b) Normalized signals of bioelectronic noses at various concentrations of geraniol in the presence and absence of 1 nM benzyl salicylate. Each point and error bar represent an average value and standard deviation for multiple experiments, respectively. The equilibrium constant between hOR1A2 and geraniol in the absence of benzyl salicylate was estimated as 8.37×10^{11} M^{-1}. In the presence of benzyl salicylate, the estimated equilibrium constant between hOR1A2 and geraniol was found to be 1.64×10^{15} M^{-1}.

Previous works show that enhancer materials such as benzyl salicylate, which occurs naturally in various plants, could enforce the richness and depth of floral compositions [49,50]. However, the effect of such

enhancers has not been evaluated quantitatively before. Here, we first performed cell-based assays to investigate whether the enhancer affects the responses of hOR1A2 in cells. Figure 3-6a is the cell assay results showing the responses of hOR1A2 to geraniol with or without an enhancer, benzyl salicylate. In brief, hOR1A2-expressing HEK-293 cells were activated by varied concentrations of geraniol in benzyl salicylate. When 0.1 μM benzyl salicylate was applied, the responses of hOR1A2 to *1*, *10* and *100 μM* geraniol were found to be enhanced by *1.63-fold*, *1.76-fold* and *1.48-fold* compared with those without the enhancer, respectively. Likewise, benzyl salicylate with a 1 μM concentration led to *2.14-fold*, *2.09-fold* and *1.52-fold* enhancement in the responses of hOR1A2 to *1*, *10* and *100 μM* geraniol, respectively. In addition, benzyl salicylate alone did not stimulate hOR1A2. These results imply that benzyl salicylate could enhance the responses of ORs to their floral scent molecules and thus enables low detection thresholds to them. Previous works show that the responses of some ORs to their odorants could be enhanced by enhancer materials such as benzyl salicylate via the allosteric modulation mechanism [51,52]. To our knowledge, this result is the first demonstration that benzyl salicylate could highly boost the responses of the cells expressing ORs to the specific odorant.

We also investigated the effect of the enhancer on the assessment of geraniol using our bioelectronic noses. Figure 3-6b shows the normalized signals of our bioelectronic noses to geraniol with or without 1 nM benzyl salicylate. First, we prepared the mixture of geraniol and benzyl salicylate, holding the concentration of benzyl salicylate at 1 nM and varying the concentrations of geraniol from 10 aM to 10 nM. Each data point was obtained by multiple measurements using four or more bioelectronic nose devices. Note that the normalized signal curve in the presence of benzyl salicylate was shifted to lower concentration regions, indicating that the bioelectronic noses began to exhibit responses at much lower concentrations of geraniol than the cases without the enhancer. We also confirmed that benzyl salicylate alone did not respond to a bare floating electrode-based CNT transducer. Following the Hill-Langmuir equation as described above, we could estimate the equilibrium constants between hOR1A2 and geraniol with or without benzyl salicylate. In the presence of 1 nM benzyl salicylate, the equilibrium constant between hOR1A2 and geraniol was estimated to be $1.64 \times 10^{15}\ M^{-1}$, while that without the enhancer was $8.37 \times 10^{11}\ M^{-1}$ in the section of Figure 3-3d. These results clearly show that benzyl salicylate contributes significantly to the enhancement of the hOR1A2 responses to geraniol and thus

decreases the thresholds of binding between hOR1A2 and geraniol. This is the first report showing that benzyl salicylate as the enhancer could affect the binding affinity of the receptor on bioelectronic devices. It also should be noted that since our method directly measured the responses of receptors without relying on complicated signal pathways like cell assays, it can be a powerful method to quantitatively evaluate the effect of enhancer materials on the binding of rose odorant molecules to receptors. Such a capability of our method could open up versatile applications in various areas such as drug, food, and cosmetic industries. We performed cell-based assays to evaluate the ligand/receptor binding activity of hOR1A2.

3.6 Quantitative Measurement of Rose Scent Ingredients in Natural Rose Oil

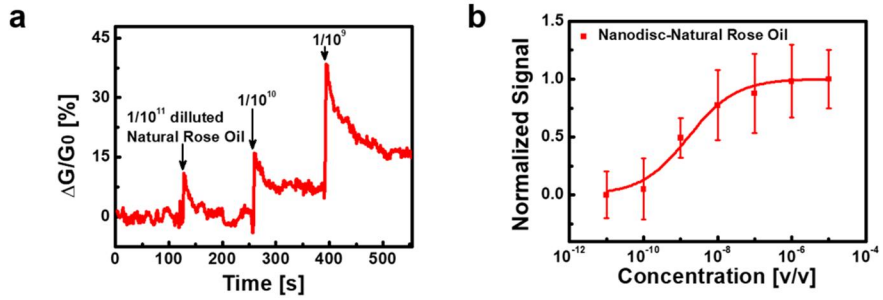

Figure 3-7 Quantitative measurement of rose scent ingredients in natural rose oil utilizing bioelectronic noses. (a) Real-time responses of a bioelectronic nose to different concentrations of natural rose oil. The introduction of the rose oil solution diluted by 10^{-11} occurred negligible responses in the conductance of the bioelectronic nose. The rose oil solutions diluted by 10^{-10} and 10^{-9} caused significant increases in the CNT-FET channel conductance. (b) Normalized signal of bioelectronic noses to natural rose oil solutions diluted from 10^{-11} to 10^{-5}. The x-axis (v/v) represents the volume/volume percent of the natural rose oil in the HEPES buffer solution. We repeated the sensing measurement using four or more bioelectronic noses to obtain average values and standard deviations.

Rose oil products extracted from roses have been utilized as base materials for versatile applications such as perfumes [53-55]. In this case, the quantitative evaluation of rose scent ingredients in rose oil can be important because the overdose of the ingredients may result in bad smells [56]. To demonstrate the validity of our method for practical

applications, we performed experiments to quantitatively evaluate rose scent ingredients in natural rose oil by utilizing our method. Figure 3-7a shows the responses of a bioelectronic nose to different concentrations of natural rose oil in real-time. The rose oil solutions were prepared by means of dilution of a natural rose oil stock solution with HEPES buffer II. The diluted rose oil solutions were consecutively introduced to the bioelectronic nose, and its responses were monitored simultaneously. The rose oil diluted by 10^{-11} caused negligible responses in the conductance of the bioelectronic nose. However, those diluted by 10^{-10} and 10^{-9} led to significant increases in the CNT-FET channel conductance. This result clearly shows that the bioelectronic nose could detect the specific rose compounds in real samples such as natural rose oil.

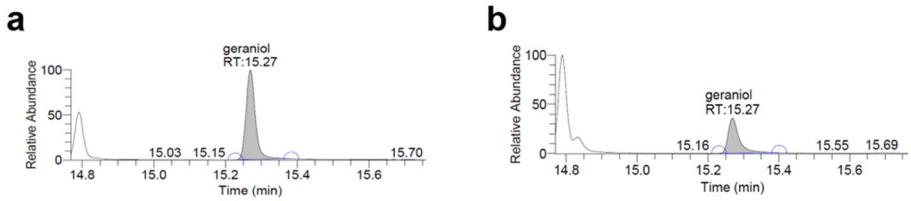

Figure 3-8 GC-MS chromatogram profiles of geraniol. (a) GC-MS chromatogram of geraniol of an authentic reference compound. Geraniol of the authentic reference compound has a peak at retention time 15.27 min. (b) GC-MS chromatogram of geraniol in natural rose oil. Geraniol in the natural

rose oil has also a peak at retention time 15.27 min. The concentration of geraniol in the undiluted natural rose oil was found to be 9.47×10^{-4} M.

Figure 3-7b shows the normalized signal of bioelectronic noses to the natural rose oil diluted for different concentrations. The rose oil stock solution was serially diluted with HEPES buffer II to prepare rose oil solutions diluted from 10^{-11} to 10^{-5}. We obtained the normalized signal of bioelectronic noses to the diluted rose oil solutions by fitting the response data in the same way as shown in Figure 3-3d. We repeated measurement for four or more bioelectronic noses to obtain quantitative results. Since the bioelectronic noses detect general species which bind to hOR1A2, our strategy can efficiently evaluate general ingredients giving a rose scent. We confirmed that geraniol could be more dominant to hOR1A2 than citronellol by the results of Figure 3-2b and Figure 3-3d. That is, hOR1A2 of the bioelectronic nose responds to geraniol mainly. This indicates that geraniol could play a dominant role in the responses of bioelectronic noses to the natural rose oil [57,58]. Then, we could estimate the concentration of geraniol in the undiluted rose oil solution by comparing $K_{rose\ oil}$ with $K_{geraniol}$, where $K_{rose\ oil}$ and $K_{geraniol}$ are the dissociation constants of hOR1A2 to the diluted rose oil and geraniol, respectively. The $K_{rose\ oil}$ was found to be

1.62×10^{-9} from the normalized signal of bioelectronic noses to the diluted rose oil solutions. Likewise, the $K_{geraniol}$ was calculated to be 1.19×10^{-12} M from the data in section of Figure 3-3d. On the basis of comparison of $K_{rose\ oil}$ to $K_{geraniol}$, we could estimate the concentration of geraniol in the undiluted rose oil as about 7.35×10^{-4} M. This value is quite close to geraniol concentration estimated by a gas chromatography mass spectrometry (GC-MS) method (Figure 3-8). The concentration of geraniol in the undiluted rose oil was estimated as 9.47×10^{-4} M by the GC-MS analysis. This means that the binding affinity of hOR1A2 with geraniol could be slightly underestimated in complicated environments containing various chemicals which could lead to lower effective concentration of geraniol to the receptor [59]. This result clearly shows that the bioelectronic noses could recognize geraniol in complex environments such as real rose oil. This result also indicates that the bioelectronic nose could be utilized for practical applications, which could open up various applications such as a stable and reliable sensor platform.

3.7 Summary

In summary, we have developed an olfactory receptor ND-based

bioelectronic nose which can smell rose scent ingredients in real samples like a human nose. In this method, we directly incorporated hOR1A2NDs onto the gold floating electrodes of a CNT-based transistor. The binding events between hOR1A2NDs and specific rose scent components were monitored electrically by the underlying CNT-FET. Using this method, we could quantitatively recognize geraniol and citronellol down to 1 fM and 10 fM, respectively. Additionally, the method allowed us to distinguish a specific rose odorant from other odorants with high selectivity. Most noticeable, our sensors were utilized to investigate the effect of the scent enhancer on the responses of ORs, and we found that the ORs in the presence of 1 nM benzyl salicylate responded to a rose scent with ~10^3 times lower concentrations. Furthermore, the method facilitated the quantitative detection of rose odorants in real rose oil just like a human nose. These results clearly show that the strategy could be a simple but powerful impetus for basic research and various applications in perfume and cosmetic industries.

3.8 References

[1] Guterman, I.; Shalit, M.; Menda, N.; Piestun, D.; Dafny-Yelin, M.; Shalev, G.; Bar, E.; Davydov, O.; Ovadis, M.; Emanuel, M.; Wang, J. H.; Adam, Z.; Pichersky, E.; Lewinsohn, E.; Zamir, D.; Vainstein, A.; Weiss, D. *Plant Cell* **2002,** *14*, 2325-2338.

[2] Babu, K. G. D.; Singh, B.; Joshi, V. P.; Singh, V. *Flavour Fragrance J.* **2002,** *17*, 136-140.

[3] Katsukawa, M.; Nakata, R.; Koeji, S.; Hori, K.; Takahashi, S.; Inoue, H. *Biosci., Biotechnol., Biochem.* **2011,** *75*, 1010-1012.

[4] Verma, R. S.; Padalia, R. C.; Chauhan, A.; Singh, A.; Yadav, A. K. *Nat. Prod. Res.* **2011,** *25*, 1577-1584.

[5] de March, C. A.; Ryu, S.; Sicard, G.; Moon, C.; Golebiowski, J. *Flavour Fragrance J.* **2015,** *30*, 342-361.

[6] Ulusoy, S.; Bosgelmez-Tinaz, G.; Secilmis-Canbay, H. *Curr Microbiol* **2009,** *59*, 554-558.

[7] Sharma, P.; Ghosh, A.; Tudu, B.; Bhuyan, L. P.; Tamuly, P.; Bhattacharyya, N.; Bandyopadhyay, R.; Das, U. *IEEE Sens. J.* **2015,** *15*, 1178-1185.

[8] Mitachi, S.; Sasaki, K.; Kondoh, M.; Sugimoto, I. *Acta Hortic.* **2005,** 113-119.

[9] Sarafoleanu, C.; Mella, C.; Georgescu, M.; Perederco, C. *J Med Life* **2009,** *2*, 196-198.

[10] Croy, I.; Negoias, S.; Novakova, L.; Landis, B. N.; Hummel, T. *PLoS One* **2012,** *7*, e33365.

[11] Malnic, B.; Hirono, J.; Sato, T.; Buck, L. B. *Cell* **1999,** *96*, 713-723.

[12] Knape, K.; Beyer, A.; Stary, A.; Buchbauer, G.; Wolschann, P. *Flavour Fragrance J* **2009,** *24*, 192-197.

[13] Oh, E. H.; Lee, S. H.; Lee, S. H.; Ko, H. J.; Park, T. H. *Biosens. Bioelectron.* **2014,** *53*, 18-25.

[14] Kwon, O. S.; Song, H. S.; Park, S. J.; Lee, S. H.; An, J. H.; Park, J. W.; Yang, H.; Yoon, H.; Bae, J.; Park, T. H.; Jang, J. *Nano Lett.* **2015,** *15*, 6559-6567.

[15] Kim, T. H.; Lee, S. H.; Lee, J.; Song, H. S.; Oh, E. H.; Park, T. H.; Hong, S. *Adv. Mater.* **2009,** *21*, 91-94.

[16] Park, S. J.; Kwon, O. S.; Lee, S. H.; Song, H. S.; Park, T. H.; Jang, J. *Nano Lett.* **2012,** *12*, 5082-5090.

[17] Yoon, H.; Lee, S. H.; Kwon, O. S.; Song, H. S.; Oh, E. H.; Park, T. H.; Jang, J. *Angew. Chem., Int. Ed. Engl.* **2009,** *48*, 2755-2758.

[18] Jin, H. J.; Lee, S. H.; Kim, T. H.; Park, J.; Song, H. S.; Park, T. H.; Hong, S. *Biosens. Bioelectron.* **2012,** *35*, 335-341.

[19] Yang, H.; Kim, D.; Kim, J.; Moon, D.; Song, H. S.; Lee, M.; Hong, S.; Park, T. H. *ACS Nano* **2017,** *11*, 11847-11855.

[20] Karyakin, A. A.; Presnova, G. V.; Rubtsova, M. Y.; Egorov, A. M. *Anal. Chem.* **2000,** *72*, 3805-3811.

[21] Lee, S. H.; Jin, H. J.; Song, H. S.; Hong, S.; Park, T. H. *J. Biotechnol.* **2012,** *157*, 467-472.

[22] Lee, M.; Jung, J. W.; Kim, D.; Ahn, Y. J.; Hong, S.; Kwon, H. W. *ACS Nano* **2015,** *9*, 11728-11736.

[23] Son, M.; Cho, D. G.; Lim, J. H.; Park, J.; Hong, S.; Ko, H. J.; Park, T. H. *Biosens. Bioelectron.* **2015,** *74*, 199-206.

[24] Zhuang, H.; Matsunami, H. *Nat. Protoc.* **2008,** *3*, 1402-1413.

[25] Schmiedeberg, K.; Shirokova, E.; Weber, H. P.; Schilling, B.; Meyerhof, W.; Krautwurst, D. *J. Struct. Biol.* **2007,** *159*, 400-412.

[26] Massberg, D.; Simon, A.; Haussinger, D.; Keitel, V.; Gisselmann,

G.; Conrad, H.; Hatt, H. *Arch. Biochem. Biophys* **2015,** *566*, 100-109.

[27] Sabouri, A. A.; Moosavimovahedi, A. A. *Biochem. Educ.* **1994,** *22*, 48-49.

[28] Ferrell, J. E., Jr. *J. Biol.* **2009,** *8*, 1-6.

[29] Franco, R. *Br. J. Pharmacol.* **2009,** *158*, 23-31.

[30] Dacres, H.; Wang, J.; Leitch, V.; Horne, I.; Anderson, A. R.; Trowell, S. C. *Biosens. Bioelectron.* **2011,** *29*, 119-124.

[31] Yang, H.; Song, H.; Ahn, S.; Park, T. *Biotechnol. Bioprocess Eng.* **2015,** *20*, 423-430.

[32] Son, M.; Kim, D.; Ko, H. J.; Hong, S.; Park, T. H. *Biosens. Bioelectron.* **2017,** *87*, 901-907.

[33] Park, S. J.; Yang, H.; Lee, S. H.; Song, H. S.; Park, C. S.; Bae, J.; Kwon, O. S.; Park, T. H.; Jang, J. *ACS Nano* **2017,** *11*, 5950-5959.

[34] Kaiser, L.; Graveland-Bikker, J.; Steuerwald, D.; Vanberghem, M.; Herlihy, K.; Zhang, S. *Proc. Natl. Acad. Sci. U. S. A.* **2008,** *105*, 15726-15731.

[35] Rouck, J. E.; Krapf, J. E.; Roy, J.; Huff, H. C.; Das, A. *FEBS Lett.* **2017,** *591*, 2057-2088.

[36] Denisov, I. G.; Baas, B. J.; Grinkova, Y. V.; Sligar, S. G. *J Biol. Chem.* **2007,** *282*, 7066-7076.

[37] Denisov, I. G.; Sligar, S. G. *Nat. Struct. Mol. Biol.* **2016,** *23*, 481-486.

[38] Whorton, M. R.; Jastrzebska, B.; Park, P. S. H.; Fotiadis, D.; Engel, A.; Palczewski, K.; Sunahara, R. K. *J. Biol. Chem.* **2008,** *283*, 4387-4394.

[39] Hollenstein, K.; de Graaf, C.; Bortolato, A.; Wang, M. W.;

Marshall, F. H.; Stevens, R. C. *Trends Pharmacol. Sci.* **2014,** *35*, 12-22.

[40] Lim, J. H.; Park, J.; Ahn, J. H.; Jin, H. J.; Hong, S.; Park, T. H. *Biosens. Bioelectron.* **2013,** *39*, 244-249.

[41] Kim, B.; Lee, J.; Namgung, S.; Kim, J.; Park, J. Y.; Lee, M. S.; Hong, S. *Sens. Actuators, B* **2012,** *169*, 182-187.

[42] Song, H. S.; Jin, H. J.; Ahn, S. R.; Kim, D.; Lee, S. H.; Kim, U. K.; Simons, C. T.; Hong, S.; Park, T. H. *ACS Nano* **2014,** *8*, 9781-9789.

[43] Park, E. J.; Park, J.; Song, H. S.; Kim, S. J.; Jung, K. C.; Kim, S. M.; Cho, D. G.; Kim, D.; Park, K. S.; Hong, S. *Biosens. Bioelectron.* **2014,** *61*, 140-146.

[44] England, C. G.; Ehlerding, E. B.; Cai, W. B. *Bioconjugate Chem.* **2016,** *27*, 1175-1187.

[45] Luker, K. E.; Luker, G. D. *Antiviral Res.* **2008,** *78*, 179-187.

[46] Kim, J. E.; Kalimuthu, S.; Ahn, B. C. *Nucl. Med. Mol. Imaging* **2015,** *49*, 3-10.

[47] Hollmann, M. W.; Strumper, D.; Herroeder, S.; Durieux, M. E. *Anesthesiology* **2005,** *103*, 1066-1078.

[48] Lerner, M. B.; D'Souza, J.; Pazina, T.; Dailey, J.; Goldsmith, B. R.; Robinson, M. K.; Johnson, A. T. *ACS Nano* **2012,** *6*, 5143-5149.

[49] Turin, L. *The secret of scent : adventures in perfume and the science of smell*; Ecco: New York, 2006.

[50] Brophy, J. J.; Goldsack, R. J.; Forster, P. I. *J. Essent. Oil Res.* **1995,** *7*, 585-588.

[51] Laskowski, R. A.; Gerick, F.; Thornton, J. M. *FEBS Lett.* **2009,** *583*, 1692-1698.

[52] Tsitoura, P.; Iatrou, K. *Front. Cell. Neurosci.* **2016,** *10*, 1-13.

[53] Kumar, A.; Nadda, G.; Shanker, A. *J. Chromatogr. A* **2004,** *1050*, 193-199.

[54] Jalali-Heravi, M.; Parastar, H.; Sereshti, H. *Anal. Chim. Acta* **2008,** *623*, 11-21.

[55] Ayci, F.; Aydinli, M.; Bozdemir, O. A.; Tutas, M. *Flavour Fragrance J.* **2005,** *20*, 481-486.

[56] Greenman, J.; El-Maaytah, M.; Duffield, J.; Spencer, P.; Rosenberg, M.; Corry, D.; Saad, S.; Lenton, P.; Majerus, G.; Nachnani, S. *J. Am. Dent. Assoc., JADA* **2005,** *136*, 749-757.

[57] Vogt, A. D.; Di Cera, E. *Biochemistry* **2013,** *52*, 5723-5729.

[58] Firestein, S. *Nature* **2001,** *413*, 211-218.

[59] Serebryany, E.; Zhu, G. A.; Yan, E. C. Y. *Biochim. Biophys. Acta* **2012,** *1818*, 225-233.

Chapter 4

Conclusions

In this dissertation, bioelectronic sensors based on CNT-FETs with floating electrodes and biomolecules were developed to monitor sensory receptor activity.

Firstly, we developed bioelectronic tongues based on naovesicles to monitor honeybee gustatory receptor activity to umami taste. Using the strategy, we quantitatively monitored the gustatory receptor (AmGr10) activity to umami taste even in real samples. The results show that the bioelectronic tongues could discriminate umami tastants with high sensitivity and selectivity. Significantly, we demonstrated that the responses of AmGr10 to MSG could be enhanced by synergism between MSG and an enhancer material. The results imply that the synergistic effect could decrease the threshold of AmGr10 response to MSG, and we could quantitatively evaluate the umami synergism using the bioelectronic tongues.

Secondly, we developed bioelectronic noses based on nanodiscs to monitor human olfactory receptor activity to a rose scent. Importantly, we quantitatively discriminated one rose scent component

from the other rose scent component. We also quantitatively evaluated the enhancing effect of an enhancer to a rose scent using the bioelectronic noses. Furthermore, the concentration of geraniol, main component of a rose scent, in real rose oil was estimated to be close to the actual concentration.

The results should contribute to broadening the understanding of various receptor activity. Further, the development of the bioelectronic sensors should provide a powerful platform mimicking real sensory systems. In addition, it is expected to be widely utilized as a practical tool for various applications in general.

Chapter 5

Abstract in Korean

초록

감각 수용체의 작용을 연구하기 위한 바이오분자-탄소나노튜브 융합 구조 및 바이오전자 센서로의 응용

인간은 후각과 미각 기관을 통해 다양한 냄새 물질과 맛 물질을 인지한다. 후각과 미각은 세포에 존재하는 감각 수용체들이 세포 밖의 화학 신호를 받아들임으로써 생성된다. 즉, 감각 수용체들이 감각 기관에서 첫번째 감지 파트로서 작용하게 된다. 따라서, 감각 수용체의 작용을 측정하는 것은 감각 기관에 대한 근본적인 이해를 위하여 필수적이다. 또한, 감각 수용체에 대한 연구는 바이오전자 센서의 개발로 이어질 수 있다. 본 연구에서는 바이오전자 센서를 통하여 감각 수용체의 작용을 전기적으로 모니터링하는 것에 대하여 논의 할 것이다. 이 바이

오전자 센서는 금으로 형성된 플로팅 전극을 가진 탄소나노튜브 전계 효과 트랜지스터를 기반으로 하고 있으며, 이는 향상된 센서 감도와 선택성을 가져온다.

먼저, 감칠맛에 대한 꿀벌의 미각 수용체의 작용을 모니터링하기 위한 나노베지클 기반 바이오 전자 미각 센서에 대하여 논의할 것이다. 이를 위하여, 플로팅 전극을 가진 탄소나노튜브 전계 효과 트랜지스터와 AmGr10 (gustatory receptor 10 of *Apis mellifera*)이라는 꿀벌의 미각 수용체를 포함하고 있는 나노베지클이 융합되었다. 이를 통해 감칠맛 물질로 잘 알려진 글루탐산 모노나트륨 (MSG)을 감칠맛을 내지 않는 물질과 높은 감도와 선택성을 가지고 구별할 수 있었다. 흥미롭게도, 이 바이오전자 미각 센서는 치킨 스톡 같은 액상 음식에 존재하는 MSG를 검지하는 데에도 이용되었다. 더욱이, 이 플랫폼을 사용하여 증강 물질 (5’-이노신산 나트륨)에 의해 감칠맛에 대한 반응이 향상됨을 보였다.

다음으로, 장미향에 대한 인간의 후각 수용체의 작용을 모니터링하기 위한 나노디스크 기반 바이오 전자 후각 센서에 관하여 논의 할 것이다. 이를 위하여, 플로팅 전극 기반의 탄

소나노튜브 전계 효과 트랜지스터가 인간 후각 수용체 1A2 (hOR1A2)가 내장된 나노디스크 (hOR1A2NDs)로 기능화되었다. 이를 통해 장미향의 주요 구성 성분인 게라니올과 시트로넬롤을 각각 1 fM과 10 fM의 낮은 농도까지 검지할 수 있었다. 우리는 또한 사람의 코처럼 장미향에 대한 hOR1A2NDs의 반응이 증강 물질에 의해 크게 향상됨을 입증하였다. 뿐만 아니라, 이 방법은 장미 오일과 같은 실제 샘플에서도 장미향 성분을 정량적으로 검출하기 위해 사용될 수도 있었다.

주요어: 감각 수용체, 나노베지클, 나노디스크, 탄소나노튜브 전계 효과 트랜지스터, 플로팅 전극, 바이오전자 센서

학번: 2013-20376